

# Scalable Beamforming Design for Multi-RIS-Aided MU-MIMO Systems with Imperfect CSIT

Mintaek Oh and Jinseok Choi

**Abstract**—This paper presents a scalable beamforming design for maximizing the spectral efficiency (SE) of multi-reconfigurable intelligent surface (RIS)-aided communications through joint optimization of the precoder and RIS phase shifts in multi-user multiple-input multiple-output (MU-MIMO) systems under imperfect channel state information at the transmitter (CSIT). To address key challenges of the joint optimization problem, we first decompose it into two subproblems by deriving a proper lower bound. We then leverage a generalized power iteration (GPI) approach to identify a superior local optimal precoding solution. We further extend this approach to the RIS design using regularization; we set a RIS regularization function to efficiently handle the unit-modulus constraints, and also find the superior local optimal solution for RIS phase shifts under the GPI-based optimization framework. Subsequently, we propose an alternating optimization method. Our proposed algorithm offers scalable multi-RIS beamforming in terms of computational complexity that scales linearly with the number of RISs, while achieving superior performance. We further reduce the complexity with respect to the number of RIS elements by using diagonal approximation of the channel error covariance and avoiding direct matrix inversion. Simulations validate the proposed algorithm in terms of both the sum SE performance and the scalability.

**Index Terms**—Reconfigurable intelligent surface, imperfect channel state information, beamforming, generalized power iteration, alternating optimization, regularization.

## I. INTRODUCTION

A reconfigurable intelligent surface (RIS) has been recognized as a promising technique for future wireless communication systems [1]. By adjusting numerous passive reflecting elements, the RIS enhances wireless channel conditions with flexible control and configuration, resulting in performance improvements with marginal increase in network power consumption. For instance, in millimeter-wave (mmWave) communications, signals can easily experience a severe attenuation due to blockage [2]. To overcome this issue, the deployment of RIS can help creating an additional signal path, thereby increasing the coverage of mmWave systems [3].

Despite the significant potential of the RIS, obtaining precise wireless channel state information (CSI) poses a considerable practical issue in RIS-aided systems [4]. This challenge is exacerbated by the fact that the passive nature of RIS does not facilitate any signal transmission, reception, or processing [5]. In addition, deploying more RISs introduces significant burden on channel estimation, which can lead to substantial performance degradation due to degraded channel estimation

accuracy. This challenge motivates us to establish beamforming strategies for RIS-aided systems with inaccurate CSI. In this regard, it is imperative to consider robust transmission design that accounts for imperfect CSI at the transmitter (CSIT) and a scalable beamforming strategy to offer a flexible beamforming solution tailored for multi-RIS-aided systems.

### A. Related Works

Because of the promising potential of utilizing the RIS, there exist various analytical works investigating multi-RIS-aided networks. Specifically, wireless networks assisted by two RISs demonstrate that the effective channel benefits from the superposition of the double-reflection link [6]. In [7], it was shown that if the double-reflection channel follows a line-of-sight (LoS) path, it can attain a higher order of passive beamforming gain compared to individual single-reflection links. The outage probability and average symbol error probability for Nakagami- $m$  fading of multi-RIS-aided systems were derived in [8]. The result in [8] indicates that multi-RIS configurations can significantly enhance diversity order and system performance. In [9], the spectral efficiency (SE) of multi-RIS-aided systems was analyzed with Poisson point processes. It was also confirmed in [10] that deploying more RISs up to an optimal number increases the network sum SE, and the optimal number can increase with proper RIS phase optimization. Overall, the literature emphasizes the potential benefit achieved by deploying multiple RISs.

Motivated by the potential of multi-RIS-aided systems, the RIS beamforming optimization has been actively investigated for multiple-input and multiple-output (MIMO) communication systems. According to [11], the problem of maximizing the weighted sum rate in a system supported by multiple RISs was tackled by jointly optimizing the precoder and RIS phase shifts. In [12], the study extended the application of RIS-aided beamforming to multi-cell networks, advancing the methodology to encompass multi-RIS systems through the aggregation of all relevant channel matrices associated with RISs. For a multiuser MIMO (MU-MIMO) downlink system, a codebook-based beamforming method was proposed to minimize transmit power while satisfying quality-of-service (QoS) constraints [13]. A recent study has also explored optimization strategies for distributed RIS architectures [14]. It is often considered that the direct link between the base station (BS) and users is not available. For instance, in [15], the RIS-aided communication system was handled through MIMO transmission by considering an upper limit for the channel capacity of the RIS for the blocked direct link scenario. In [3], the hybrid beamforming design was proposed in the RIS-assisted point-to-point MIMO system without the consideration of the direct

M. Oh and J. Choi are with the School of Electrical Engineering, Korea Advanced Institute of Science and Technology (KAIST), Daejeon, 34141, Republic of Korea (e-mail: {ohmin, jinseok}@kaist.ac.kr).

link. In addition, the RIS can play a pivotal role in supporting various next-generation wireless communication systems, such as integrated sensing and communication as well as low-Earth orbit satellites [16]–[18]. Therefore, a comprehensive beamforming optimization framework is indispensable for a general multi-RIS-aided system to fully leverage these diverse applications and maximize system performance.

Considering the difficulty in channel estimation for the RIS-aided system, robust beamforming approaches have been proposed to compensate for channel estimation inaccuracies [19]–[23]. Moreover, advanced mathematical frameworks for channel estimation [24] have been developed, broadening the scope of robust system design. In [19], a robust beamforming design was proposed to minimize transmit power under worst-case rate constraints with imperfect CSIT of cascaded channels. The study found that substantial channel estimation errors can significantly degrade overall system performance, and provided engineering insights for the size of the RIS when dealing with imperfect CSIT. In [23], it was emphasized that precise channel estimation is crucial in achieving maximum fairness and QoS for multi-group systems, noting that deploying RIS may not yield performance gains and could potentially degrade system performance without accurate CSI.

Although several approaches have been successfully proposed by employing famous optimization frameworks such as manifold optimization and successive convex approximation techniques [12], [21], [25]–[31], most approaches have achieved sub-optimal solutions, leaving a room for further performance improvement. In addition, some of the proposed approaches have limited scalability for multiple RISs in terms of the computational complexity. Specifically, in [12], [28], [32], manifold optimization (MO)-based algorithm and a majorization-minimization (MM)-based algorithm yield sub-optimal performance due to the inherently non-convex nature of the optimization problems. Moreover, regarding the number of RISs  $L$ , the high-performing algorithms' complexity increases in the order of  $O(L^2)$  or even higher [11], [13], [31]. Therefore, there is a need for more effective and scalable beamforming designs tailored for multi-RIS-aided systems which can surpass existing sub-optimal and high-complexity methods, especially for imperfect CSIT scenarios.

## B. Contributions

We investigate multi-RIS-aided MU-MIMO downlink systems with imperfect CSIT. Specifically, we propose a novel optimization framework that jointly optimizes the precoder and RIS phase shifts with achieving scalability in both the number of RISs and their elements, significantly advancing the state of the art. The main contributions are summarized as follows:

- In the considered system, we assume that estimated channels and their estimation error covariance are known at the BS. Under this assumption, we adopt the instantaneous SE to fully exploit the available channel knowledge, which is desirable to maximize the performance gain. This instantaneous SE is the short-term SE expression that averages over channel estimation error distribution.

To make this metric tractable, we derive a lower bound of the instantaneous SE. Consequently, our metric involves the channel error covariance as well as the estimated channel, allowing us to exploit the partial CSIT. Based on this approach, we can achieve a robust solution aiming at maximizing the sum SE under imperfect CSIT.

- Based on the derived instantaneous SE bound, we first optimize the precoder based on a generalized power iteration (GPI) method [33]. To this end, we begin with decomposing the problem into two subproblems: (i) the precoder optimization and (ii) the RIS phase shifts optimization. Subsequently, deriving the first-order optimality condition for the precoder with given RIS phase shifts, we interpret the precoding optimization problem as a generalized eigenvalue problem. Subsequently, applying the GPI method, we find the superior local optimal precoding solution that is a principal eigenvector.
- Regarding RIS phase shifts, we develop a regularized GPI method to effectively resolve the unit-modulus constraint and achieve multi-RIS scalability by utilizing a block-diagonal structure in the GPI method. Introducing a regularization term as a function of RIS phase shifts, the unit-modulus condition is controlled by the regularization function without the explicit constraint. Through smooth approximation and GPI-friendly reformulation of the problem, we apply the GPI method, ultimately achieving superior local optimal solution.
- By leveraging block-diagonal matrices of the GPI framework, the overall complexity becomes lower compared to state-of-the-art methods. In particular, our approach enables scalable beamforming by reducing the computational complexity to a linear growth with the number of RISs, i.e.,  $O(L)$ . We further reduce the complexity with respect to the number of RIS elements by using diagonal approximation of the channel error covariance and avoiding direct matrix inversion.
- Via simulations, we demonstrate that our proposed method outperforms baselines across various scenarios, achieving superior local solutions. We also empirically confirm that the regularized GPI approach nearly satisfies the unit-modulus constraint, which verifies the effectiveness of our regularized GPI approach. In addition, we show that our method exhibits its multi-RIS scalability while achieving the highest sum SE.

*Notation:* The superscripts  $(\cdot)^T$ ,  $(\cdot)^H$ ,  $(\cdot)^*$ , and  $(\cdot)^{-1}$  denote the transpose, Hermitian, complex conjugate, and matrix inversion, respectively.  $\mathbf{I}_N$  is the identity matrix of size  $N \times N$  and  $\mathbf{0}$  is a zero vector with proper dimension. We use  $\text{diag}(\mathbf{a})$  for a diagonal matrix with  $\mathbf{a}$  on its diagonal elements. Assuming that  $\mathbf{A}_1, \dots, \mathbf{A}_N \in \mathbb{C}^{K \times K}$ ,  $\mathbf{A} = \text{blkdiag}(\mathbf{A}_1, \dots, \mathbf{A}_N) \in \mathbb{C}^{KN \times KN}$  is a block-diagonal matrix.  $\|\mathbf{A}\|$  represents L2 norm. We use  $\text{tr}(\cdot)$  for trace operator,  $\text{vec}(\cdot)$  for vectorization,  $\otimes$  for Kronecker product, and  $\arg(\cdot)$  for the argument of a complex number. With mean  $m$  and variance  $\sigma^2$ , we use  $\mathcal{CN}(m, \sigma^2)$  for a circularly symmetric complex Gaussian distribution and  $\mathcal{N}(m, \sigma^2)$  for a Gaussian distribution.

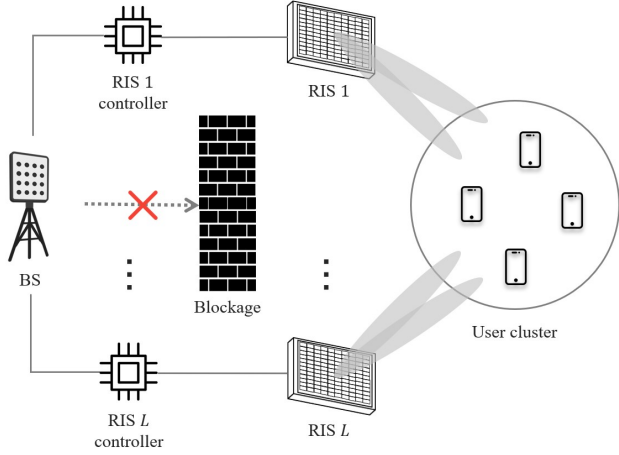


Fig. 1. An illustration of the multi-RIS-aided downlink MU-MIMO system architecture.

## II. SYSTEM MODEL AND PROBLEM FORMULATION

### A. Signal Model

As shown in Fig. 1, we consider a multi-RIS-aided MU-MIMO downlink system where the BS equipped with  $N$  antennas serves  $K$  single-antenna users assisted with  $L$  RISs. Each RIS is equipped with  $M$  reflecting elements:  $\Phi_\ell = \text{diag}(\phi_\ell)$  where  $\phi_\ell = [\phi_{1,\ell}, \phi_{2,\ell}, \dots, \phi_{M,\ell}]^T$  with  $\phi_{m,\ell} = e^{j\theta_{m,\ell}}, \forall m, \forall \ell$ . We denote the user set, RIS set, and set of indices of RIS reflecting elements as  $\mathcal{K} = \{1, \dots, K\}$ ,  $\mathcal{L} = \{1, \dots, L\}$ , and  $\mathcal{M} = \{1, \dots, M\}$ , respectively. The BS determines the optimal phase shifts and conveys the information back to the corresponding RIS controller. Assuming that the RIS is deployed in the vicinity of the BS, the control signaling can be implemented by an error-free link with negligible latency via wired links [34]. The BS broadcasts the data symbols  $s_k \sim \mathcal{CN}(0, P), \forall k \in \mathcal{K}$  to each legitimate user via a precoder  $\mathbf{F} = [\mathbf{f}_1, \dots, \mathbf{f}_K] \in \mathbb{C}^{N \times K}$  where  $\mathbf{f}_k \in \mathbb{C}^N$  indicates a precoding vector for  $s_k$ . Then, a transmitted signal vector is given by

$$\mathbf{x} = \sum_{k=1}^K \mathbf{f}_k s_k = \mathbf{F}\mathbf{s} \in \mathbb{C}^N, \quad (1)$$

where  $\mathbf{s} = [s_1, \dots, s_K]^T \in \mathbb{C}^K$ .

Let  $\mathbf{H}_{1,\ell} \in \mathbb{C}^{N \times M}$  and  $\mathbf{H}_{2,\ell} \in \mathbb{C}^{M \times K}$  denote an  $\ell$ th BS-RIS channel matrix and a  $\ell$ th RIS-user channel matrix, respectively. For the link between RIS  $\ell$  and user  $k$ , we consider  $\mathbf{h}_{2,k,\ell} \in \mathbb{C}^M$  based on a user channel matrix  $\mathbf{H}_{2,\ell} = [\mathbf{h}_{2,1,\ell}, \dots, \mathbf{h}_{2,K,\ell}]$ . We assume that the direct link between transmitter and receiver is not available. The systems assisted by multiple RISs often ignore secondary reflections between the surfaces, which is a reasonable oversight when the RISs are in each other's far-field. Thus, we assume a far-field propagation model<sup>1</sup> so that the double-reflection link can be

<sup>1</sup>In multi-RIS scenarios, inter-RIS interference from double-reflection links may occur. However, compounded pathloss factors substantially attenuate the inter-RIS interference gain relative to the primary links. This theoretical insight justifies our assumption as both analytically tractable and practically acceptable for multi-RIS-aided systems.

ignored [28]. Accordingly, a received signal at user  $k$  is given by

$$y_k = \left( \sum_{\ell=1}^L \mathbf{H}_{1,\ell} \Phi_\ell \mathbf{h}_{2,k,\ell} \right)^H \mathbf{f}_k s_k + \sum_{i=1, i \neq k}^K \left( \sum_{\ell=1}^L \mathbf{H}_{1,\ell} \Phi_\ell \mathbf{h}_{2,k,\ell} \right)^H \mathbf{f}_i s_i + n_k, \quad (2)$$

where  $n_k \sim \mathcal{CN}(0, \sigma^2)$  is additive white Gaussian noise (AWGN) of the  $k$ th user.

Now, let us define the effective channel matrix between the BS and the  $K$  users as

$$\mathbf{H} = \sum_{\ell=1}^L \mathbf{H}_{1,\ell} \Phi_\ell \mathbf{H}_{2,\ell} = [\mathbf{h}_1, \dots, \mathbf{h}_K]. \quad (3)$$

Then denoting the cascaded channel for user  $k$  at RIS  $\ell$  as  $\mathbf{H}_{k,\ell}^r = \mathbf{H}_{1,\ell} \text{diag}(\mathbf{h}_{2,k,\ell}) \in \mathbb{C}^{N \times M}$ , we rewrite the effective channel vector of user  $k$  as

$$\mathbf{h}_k = \sum_{\ell=1}^L \mathbf{H}_{1,\ell} \Phi_\ell \mathbf{h}_{2,k,\ell} = \sum_{\ell=1}^L \mathbf{H}_{k,\ell}^r \phi_\ell. \quad (4)$$

We consider a block fading model where the channel is invariant within each transmission block.

### B. Channel Acquisition Model

We assume that the BS performs uplink channel estimation and thus, the BS only has partial knowledge of the channels due to estimation imperfections. In [28], [35], the RIS channel estimation is implemented for the cascaded channel under a time-division duplex mode. For the cascaded channel, the estimated CSIT is given by

$$\hat{\mathbf{H}}_{k,\ell}^r = \mathbf{H}_{k,\ell}^r - \mathbf{E}_{k,\ell}, \quad (5)$$

or equivalently in a vectorized form, we have

$$\hat{\mathbf{c}}_{k,\ell} = \mathbf{c}_{k,\ell} - \mathbf{e}_{k,\ell}, \quad (6)$$

where  $\mathbf{E}_{k,\ell}$  is a channel estimation error matrix,  $\hat{\mathbf{c}}_{k,\ell} = \text{vec}(\hat{\mathbf{H}}_{k,\ell}^r)$ ,  $\mathbf{c}_{k,\ell} = \text{vec}(\mathbf{H}_{k,\ell}^r)$ , and  $\mathbf{e}_{k,\ell} = \text{vec}(\mathbf{E}_{k,\ell})$ .

According to [28], using the linear minimum mean square error (LMMSE) estimator with  $T_{\text{UL}}$  uplink training length, the error covariance matrix is given by

$$\mathbf{R}_{k,\ell}^e = \mathbb{E} \left[ \mathbf{e}_{k,\ell} \mathbf{e}_{k,\ell}^H \right] = \left( \mathbf{C}_{k,\ell}^{-1} + \frac{\rho_{\text{UL}}}{\gamma_{k,\ell} \sigma^2} \Psi_\ell^H \Psi_\ell \otimes \mathbf{I}_N \right)^{-1}, \quad (7)$$

where  $\rho_{\text{UL}}$  is uplink training power,  $\mathbf{C}_{k,\ell}$  is the cascaded channel covariance matrix,  $\Psi_\ell$  is the training phase shift matrix of  $\ell$ th RIS, and  $\gamma_{k,\ell}$  denotes the pathloss of the cascaded channel determined by  $\gamma_{k,\ell} = \gamma_{1,\ell} \gamma_{2,k,\ell}$  where  $\gamma_{1,\ell}$  and  $\gamma_{2,k,\ell}$  are the pathloss of the  $\ell$ th RIS-BS and RIS-user  $k$ , respectively. While the error covariance matrix in (7) remains unaffected by the choice of training signals, the performance of channel estimation is influenced by other factors, particularly the pattern of  $\Psi_\ell$ . Hence, careful design of an appropriate training matrix  $\Psi_\ell$  is crucial for optimizing the channel estimation process. In this paper, we adopt the discrete Fourier

transform (DFT)-based training scheme [35]. With the DFT scheme, the error covariance matrix is given by

$$\mathbf{R}_{k,\ell}^e = \left( \mathbf{C}_{k,\ell}^{-1} + \frac{T_{UL}\rho_{UL}}{\gamma_{k,\ell}\sigma^2} \mathbf{I}_{NM} \right)^{-1}, \quad (8)$$

where the sequence length for channel training needs to satisfy  $T_{UL} \geq M$ . As the uplink training length and power increase to infinity, the error covariance in (8) goes to zero; thereby the CSIT error eventually vanishes.

In the presence of multiple RISs, we assume the on-off scheme [28], [36] for each individual RIS, where each RIS is independently switched on and off by exploiting reflection and absorption characteristics of its elements [37]. Specifically, the  $\ell$ th cascaded channel is estimated while turning off all reflecting elements of RISs related to other cascaded channels. Then, each cascaded channel estimation process is divided into  $M$  stages in which each stage only estimates one column vector of  $\hat{\mathbf{H}}_{k,\ell}^r$  [38]. Once the channel estimation is completed, all cascaded channels are combined to obtain (4) for all users. We adopt this channel estimation scheme with the LMMSE estimator by taking advantage of leveraging the error covariance matrix in (8) for our system.

### C. Performance Metrics and Problem Formulation

With the effective channel in (4), the SE of user  $k$  is

$$R_k = \log_2 \left( 1 + \frac{|\mathbf{h}_k^H \mathbf{f}_k|^2}{\sum_{i=1, i \neq k}^K |\mathbf{h}_k^H \mathbf{f}_i|^2 + \frac{\sigma^2}{P}} \right). \quad (9)$$

Unfortunately, the BS cannot predict the SE in (9) for imperfect CSI. To overcome this, we consider the instantaneous SE defined as  $\mathbb{E}_{\{\hat{\mathbf{H}}_{k,\ell}^r, \hat{\mathbf{H}}_{k,\ell}^r\}}[R_k | \hat{\mathbf{H}}_{k,\ell}^r]$  [39], [40]. While an ergodic SE represents the long-term SE achievable when channel coding spans extensive channel blocks, the instantaneous SE refers to the short-term SE expression that averages channel estimation error distribution in each channel realization. We exploit the instantaneous SE to express the ergodic SE in our problem with imperfect CSIT.

According to [39], the ergodic SE of user  $k$  is defined as

$$\begin{aligned} \mathbb{E}_{\{\mathbf{h}_k\}}[R_k] &= \mathbb{E}_{\{\mathbf{H}_{k,\ell}, \hat{\mathbf{H}}_{k,\ell}^r\}}[R_k] \\ &= \mathbb{E}_{\{\hat{\mathbf{H}}_{k,\ell}^r\}} \left[ \mathbb{E}_{\{\mathbf{H}_{k,\ell}\}}[R_k | \hat{\mathbf{H}}_{k,\ell}^r] \right] \\ &= \mathbb{E}_{\{\hat{\mathbf{H}}_{k,\ell}^r\}} \left[ R_k^{\text{ins}} \right], \end{aligned} \quad (10)$$

where the expectation is taken over the randomness associated with the imperfect knowledge of the channel fading process and  $R_k^{\text{ins}}$  is the instantaneous SE. From (10), we define this instantaneous SE as

$$R_k^{\text{ins}} = \mathbb{E}_{\{\mathbf{E}_{k,\ell}\}} \left[ \log_2 \left( 1 + \frac{\left| \left( \sum_{\ell=1}^L \mathbf{H}_{k,\ell}^r \boldsymbol{\phi}_\ell \right)^H \mathbf{f}_k \right|^2}{\sum_{i=1, i \neq k}^K \left| \left( \sum_{\ell=1}^L \mathbf{H}_{k,\ell}^r \boldsymbol{\phi}_\ell \right)^H \mathbf{f}_i \right|^2 + \frac{\sigma^2}{P}} \right) \right] \hat{\mathbf{H}}_{k,\ell}^r. \quad (11)$$

However, (11) is still not tractable because there exists no closed-form expression for the expectation of the CSIT error.

To achieve a closed-form expression for the instantaneous SE, we introduce the following proposition.

**Proposition 1.** *Using the LMMSE estimator, we consider all channel estimation errors as uncorrelated noise with the transmitted signal. Accordingly, the lower bound of the instantaneous SE is derived as*

$$\begin{aligned} R_k^{\text{ins}} &\geq \log_2 \left( 1 + \frac{\left| \left( \sum_{\ell=1}^L \hat{\mathbf{H}}_{k,\ell}^r \boldsymbol{\phi}_\ell \right)^H \mathbf{f}_k \right|^2}{\sum_{i=1, i \neq k}^K \left| \left( \sum_{\ell=1}^L \hat{\mathbf{H}}_{k,\ell}^r \boldsymbol{\phi}_\ell \right)^H \mathbf{f}_i \right|^2 + \sum_{i=1}^K \mathbf{f}_i^H \boldsymbol{\Xi}_k \mathbf{f}_i + \frac{\sigma^2}{P}} \right) \\ &= \bar{R}_k^{\text{ins}}(\mathbf{F}, \boldsymbol{\Phi}), \end{aligned} \quad (12)$$

where  $\boldsymbol{\Xi}_k = \sum_{\ell=1}^L \left( \boldsymbol{\phi}_\ell^T \otimes \mathbf{I}_N \right) \mathbf{R}_{k,\ell}^e \left( \boldsymbol{\phi}_\ell^T \otimes \mathbf{I}_N \right)^H$ .

*Proof.* Using the LMMSE estimator, we can treat channel estimation errors as uncorrelated noise:

$$\begin{aligned} y_k &= \left( \sum_{\ell=1}^L \hat{\mathbf{H}}_{k,\ell}^r \boldsymbol{\phi}_\ell \right)^H \mathbf{f}_k s_k + \sum_{i=1, i \neq k}^K \left( \sum_{\ell=1}^L \hat{\mathbf{H}}_{k,\ell}^r \boldsymbol{\phi}_\ell \right)^H \mathbf{f}_i s_i \\ &\quad + \underbrace{\sum_{i=1}^K \left( \sum_{\ell=1}^L \mathbf{E}_{k,\ell} \boldsymbol{\phi}_\ell \right)^H \mathbf{f}_i s_i}_{\text{uncorrelated errors}} + n_k. \end{aligned} \quad (13)$$

Then, the lower bound of the instantaneous SE is derived by the following procedure from (14) to (16) at top of the next page. Specifically, (a) in (14) is obtained by treating the channel estimation error as worst-case uncorrelated additive Gaussian noise. According to [41], under the uncorrelation condition, the worst-case noise that minimizes mutual information for a given covariance is Gaussian, leading to the worst-case capacity expression in the form of (14). For (b) in (15), we use Jensen's inequality<sup>2</sup>. For (c) in (16), we apply the vectorization, i.e.,  $\text{vec}(\mathbf{A}\mathbf{B}) = (\mathbf{B}^T \otimes \mathbf{I}_a) \text{vec}(\mathbf{A})$  with  $\mathbf{A} \in \mathbb{C}^{a \times b}$  and  $\mathbf{B} \in \mathbb{C}^{b \times c}$ , to obtain  $\mathbf{E}_{k,\ell} \boldsymbol{\phi}_\ell = (\boldsymbol{\phi}_\ell^T \otimes \mathbf{I}_N) \mathbf{e}_{k,\ell}$ , and then express the channel estimation error term as its covariance matrix  $\mathbf{R}_{k,\ell}^e$ . Using this result, we can then calculate the expectation across all channel error terms in the second term of the denominator in (14) as  $\mathbb{E} \left[ \left( \boldsymbol{\phi}_\ell^T \otimes \mathbf{I}_N \right) \mathbf{e}_{k,\ell} \mathbf{e}_{k,\ell}^H \left( \boldsymbol{\phi}_\ell^T \otimes \mathbf{I}_N \right)^H \right] = \left( \boldsymbol{\phi}_\ell^T \otimes \mathbf{I}_N \right) \mathbf{R}_{k,\ell}^e \left( \boldsymbol{\phi}_\ell^T \otimes \mathbf{I}_N \right)^H$ ,  $\forall \ell, k$ . This completes the proof. ■

Thanks to the expression in (12), we are able to leverage the partial channel knowledge, i.e., the channel estimate and its error covariance. Aiming to maximize the sum SE by jointly optimizing the precoder and RIS phase shifts, we formulate the optimization problem with (12) as

$$\text{maximize}_{\mathbf{f}_1, \dots, \mathbf{f}_K, \boldsymbol{\Phi}} \sum_{k=1}^K \bar{R}_k^{\text{ins}}(\mathbf{F}, \boldsymbol{\Phi}) \quad (17)$$

$$\text{subject to} \sum_{k=1}^K \|\mathbf{f}_k\|^2 \leq 1, \quad (18)$$

$$|\phi_{\ell,m}| = 1, \quad \forall \ell \in \mathcal{L}, \forall m \in \mathcal{M}, \quad (19)$$

<sup>2</sup>When the number of BS antennas  $N$  is sufficiently large, the gap between the exact SE and the Jensen's bound becomes negligible, making our bound a robust and reasonable approximation for large-scale MIMO systems [42].

$$\mathbb{E}_{\{\hat{\mathbf{H}}_{k,\ell}^r\}} \left[ \mathbf{R}_k^{\text{ins}} \right] \stackrel{(a)}{\geq} \mathbb{E}_{\{\hat{\mathbf{H}}_{k,\ell}^r\}} \left[ \mathbb{E}_{\{\mathbf{E}_{k,\ell}\}} \left[ \log_2 \left( 1 + \frac{\left| \left( \sum_{\ell=1}^L \hat{\mathbf{H}}_{k,\ell}^r \boldsymbol{\phi}_\ell \right)^H \mathbf{f}_k \right|^2}{\sum_{i=1, i \neq k}^K \left| \left( \sum_{\ell=1}^L \hat{\mathbf{H}}_{k,\ell}^r \boldsymbol{\phi}_\ell \right)^H \mathbf{f}_i \right|^2 + \sum_{i=1}^K \left| \left( \sum_{\ell=1}^L \hat{\mathbf{E}}_{k,\ell} \boldsymbol{\phi}_\ell \right)^H \mathbf{f}_i \right|^2 + \frac{\sigma^2}{P}} \right) \right] \hat{\mathbf{H}}_{k,\ell}^r \right] \quad (14)$$

$$\stackrel{(b)}{\geq} \mathbb{E}_{\{\hat{\mathbf{H}}_{k,\ell}^r\}} \left[ \log_2 \left( 1 + \frac{\left| \left( \sum_{\ell=1}^L \hat{\mathbf{H}}_{k,\ell}^r \boldsymbol{\phi}_\ell \right)^H \mathbf{f}_k \right|^2}{\sum_{i=1, i \neq k}^K \left| \left( \sum_{\ell=1}^L \hat{\mathbf{H}}_{k,\ell}^r \boldsymbol{\phi}_\ell \right)^H \mathbf{f}_i \right|^2 + \mathbb{E}_{\{\mathbf{E}_{k,\ell}\}} \left[ \sum_{i=1}^K \mathbf{f}_i^H \left( \sum_{\ell=1}^L \mathbf{E}_{k,\ell} \boldsymbol{\phi}_\ell \boldsymbol{\phi}_\ell^H \mathbf{E}_{k,\ell}^H \right) \mathbf{f}_i \right] + \frac{\sigma^2}{P}} \right) \right] \quad (15)$$

$$\stackrel{(c)}{=} \mathbb{E}_{\{\hat{\mathbf{H}}_{k,\ell}^r\}} \left[ \log_2 \left( 1 + \frac{\left| \left( \sum_{\ell=1}^L \hat{\mathbf{H}}_{k,\ell}^r \boldsymbol{\phi}_\ell \right)^H \mathbf{f}_k \right|^2}{\sum_{i=1, i \neq k}^K \left| \left( \sum_{\ell=1}^L \hat{\mathbf{H}}_{k,\ell}^r \boldsymbol{\phi}_\ell \right)^H \mathbf{f}_i \right|^2 + \sum_{i=1}^K \mathbf{f}_i^H \sum_{\ell=1}^L \left( \boldsymbol{\phi}_\ell^T \otimes \mathbf{I}_N \right) \mathbf{R}_{k,\ell}^e \left( \boldsymbol{\phi}_\ell^T \otimes \mathbf{I}_N \right)^H \mathbf{f}_i + \frac{\sigma^2}{P}} \right) \right] \quad (16)$$

where  $\boldsymbol{\Phi} = [\boldsymbol{\Phi}_1, \boldsymbol{\Phi}_2, \dots, \boldsymbol{\Phi}_L] \in \mathbb{C}^{M \times LM}$ . Since (17) is non-convex, it is challenging to obtain the globally optimal solution. Additionally, the non-convex unit-modulus constraint in (19) further aggravates the challenge. These characteristics render the joint optimization of precoding and RIS phase shifts a highly challenging task. Thus, it is necessary to establish the efficient optimization framework to tackle the problem.

### III. PROPOSED BEAMFORMING DESIGN

In this section, we aim to maximize the sum SE by solving the joint optimization problem in (17). To this end, we propose a joint optimization framework that decomposes the problem into two subproblems: (i) the precoder  $\mathbf{F}$  optimization and (ii) the RIS phase shifts  $\boldsymbol{\Phi}$  optimization. We then solve these subproblems in an alternating manner under a unified framework to identify a superior local optimal solution. Although this alternating strategy is inherently iterative and adds additional complexity, it is indispensable for decomposing the non-convex joint optimization problem into tractable subproblems. Beyond the specific application to our system model, this approach has been widely validated, consistently yielding effective, high-quality solutions [25], [28].

#### A. Optimizing Precoder $\mathbf{F}$

In this subsection, we optimize the precoder  $\mathbf{F}$  while fixing the RIS phase shifts  $\boldsymbol{\Phi}$ . To highlight this, we omit the notation  $\boldsymbol{\Phi}$  from  $\bar{\mathbf{R}}_k^{\text{ins}}(\mathbf{F}, \boldsymbol{\Phi})$  and thus, we have

$$\underset{\mathbf{f}_1, \dots, \mathbf{f}_K}{\text{maximize}} \sum_{k=1}^K \bar{\mathbf{R}}_k^{\text{ins}}(\mathbf{F}) \quad (20)$$

$$\text{subject to} \sum_{k=1}^K \|\mathbf{f}_k\|^2 \leq 1. \quad (21)$$

Thanks to the reformulation of the original problem with the lower bound of instantaneous SE in (12), we can utilize the GPI approach in [33]. To adopt the method, we first vectorize the precoding matrix as

$$\bar{\mathbf{f}} = \text{vec}(\mathbf{F}) = [\mathbf{f}_1^T, \mathbf{f}_2^T, \dots, \mathbf{f}_K^T]^T \in \mathbb{C}^{NK}. \quad (22)$$

Considering the maximum transmit power  $P$ , we set  $\|\bar{\mathbf{f}}\|^2 = 1$  to achieve the maximum sum SE. With the estimated cascaded channel of user  $k$  denoted as  $\hat{\mathbf{h}}_k = \sum_{\ell=1}^L \hat{\mathbf{H}}_{k,\ell}^r \boldsymbol{\phi}_\ell$ , we replace

$\frac{\sigma^2}{P}$  with  $\frac{\sigma^2}{P} \|\mathbf{f}\|^2$  in (12), and rewrite the problem in (20) into more tractable expression, the function of Rayleigh quotient form, as

$$\underset{\bar{\mathbf{f}}}{\text{maximize}} \sum_{k=1}^K \log_2 \left( \frac{\bar{\mathbf{f}}^H \mathbf{A}_k \bar{\mathbf{f}}}{\bar{\mathbf{f}}^H \mathbf{B}_k \bar{\mathbf{f}}} \right), \quad (23)$$

where

$$\mathbf{A}_k = \text{blkdiag} \left( \hat{\mathbf{h}}_k \hat{\mathbf{h}}_k^H + \boldsymbol{\Xi}_k, \dots, \hat{\mathbf{h}}_k \hat{\mathbf{h}}_k^H + \boldsymbol{\Xi}_k \right) + \mathbf{I}_{NK} \frac{\sigma^2}{P}, \quad (24)$$

$$\mathbf{B}_k = \mathbf{A}_k - \text{blkdiag} \left( \mathbf{0}, \dots, \hat{\mathbf{h}}_k \hat{\mathbf{h}}_k^H, \dots, \mathbf{0} \right). \quad (25)$$

The second term on the right hand side in (25) has a nonzero block located at the  $k$ th block entry. We can ignore the transmit power constraint (18) because of  $\|\bar{\mathbf{f}}\|^2 = 1$  and scaling invariance of  $\bar{\mathbf{f}}$  in (23). For simplicity, we define the objective function in (23) as

$$\mathcal{L}_{\text{BS}}(\bar{\mathbf{f}}) = \log_2 \prod_{k=1}^K \left( \frac{\bar{\mathbf{f}}^H \mathbf{A}_k \bar{\mathbf{f}}}{\bar{\mathbf{f}}^H \mathbf{B}_k \bar{\mathbf{f}}} \right) = \log_2 \lambda_{\text{BS}}(\bar{\mathbf{f}}). \quad (26)$$

Then, we derive Lemma 1 to find the stationary points of (26).

**Lemma 1.** *The stationary condition of the problem (23) is satisfied if the following holds:*

$$\bar{\mathbf{B}}^{-1}(\bar{\mathbf{f}}) \bar{\mathbf{A}}(\bar{\mathbf{f}}) \bar{\mathbf{f}} = \lambda_{\text{BS}}(\bar{\mathbf{f}}) \bar{\mathbf{f}}, \quad (27)$$

where

$$\bar{\mathbf{A}}(\bar{\mathbf{f}}) = \lambda_{\text{BS,num}}(\bar{\mathbf{f}}) \sum_{k=1}^K \left( \frac{\mathbf{A}_k}{\bar{\mathbf{f}}^H \mathbf{A}_k \bar{\mathbf{f}}} \right), \quad (28)$$

$$\bar{\mathbf{B}}(\bar{\mathbf{f}}) = \lambda_{\text{BS,den}}(\bar{\mathbf{f}}) \sum_{k=1}^K \left( \frac{\mathbf{B}_k}{\bar{\mathbf{f}}^H \mathbf{B}_k \bar{\mathbf{f}}} \right), \quad (29)$$

and  $\lambda_{\text{BS,num}}(\bar{\mathbf{f}})$  and  $\lambda_{\text{BS,den}}(\bar{\mathbf{f}})$  are any functions that meet  $\lambda_{\text{BS}}(\bar{\mathbf{f}}) = \lambda_{\text{BS,num}}(\bar{\mathbf{f}}) / \lambda_{\text{BS,den}}(\bar{\mathbf{f}})$ .

*Proof.* Please refer to Appendix A. ■

We note that the stationary condition in (27) can be interpreted as a generalized eigenvalue problem. Here,  $\lambda_{\text{BS}}(\bar{\mathbf{f}})$  is an eigenvalue of  $\bar{\mathbf{B}}^{-1}(\bar{\mathbf{f}}) \bar{\mathbf{A}}(\bar{\mathbf{f}})$  with  $\bar{\mathbf{f}}$  as a corresponding eigenvector. As a result, maximizing the objective function  $\mathcal{L}_{\text{BS}}(\bar{\mathbf{f}})$  is equivalent to maximizing  $\lambda_{\text{BS}}(\bar{\mathbf{f}})$ . Therefore, it is desirable to find the principal eigenvalue of (27) to maximize

---

**Algorithm 1: GPI-Based Precoding Algorithm**


---

**1 initialize:**  $\mathbf{F}^{(0)}$ .  
**2** Set  $\bar{\mathbf{f}}^{(0)} = \text{vec}(\mathbf{F}^{(0)})$  and  $t = 1$ .  
**3 while**  $\|\bar{\mathbf{f}}^{(t)} - \bar{\mathbf{f}}^{(t-1)}\| > \varepsilon_1$  or  $t \leq t_{1,\max}$  **do**  
**4** Build  $\bar{\mathbf{A}}(\bar{\mathbf{f}}^{(t-1)})$  and  $\bar{\mathbf{B}}(\bar{\mathbf{f}}^{(t-1)})$  according to (28)  
and (29) for given  $\Phi$ .  
**5** Compute  $\bar{\mathbf{f}}^{(t)} = \bar{\mathbf{B}}^{-1}(\bar{\mathbf{f}}^{(t-1)})\bar{\mathbf{A}}(\bar{\mathbf{f}}^{(t-1)})\bar{\mathbf{f}}^{(t-1)}$ .  
**6** Normalize  $\bar{\mathbf{f}}^{(t)} = \bar{\mathbf{f}}^{(t)} / \|\bar{\mathbf{f}}^{(t)}\|$ .  
**7**  $t \leftarrow t + 1$ .  
**8 return**  $\mathbf{F}^* \leftarrow \bar{\mathbf{f}}^{(t)}$ .

---

(26), which is equivalent to finding the superior local optimal solution of (20). Based on (27), we propose the sum SE maximization precoding algorithm by employing the GPI method [33], [43] As described in Algorithm 1, we first initialize  $\bar{\mathbf{f}}^{(0)}$  and update  $\bar{\mathbf{f}}^{(t)}$  at each iteration with given  $\Phi$ ; the algorithm computes  $\bar{\mathbf{A}}(\bar{\mathbf{f}}^{(t-1)})$  and  $\bar{\mathbf{B}}(\bar{\mathbf{f}}^{(t-1)})$  according to (28) and (29). Then, the algorithm updates  $\bar{\mathbf{f}} \leftarrow \bar{\mathbf{B}}^{-1}(\bar{\mathbf{f}}^{(t-1)})\bar{\mathbf{A}}(\bar{\mathbf{f}}^{(t-1)})\bar{\mathbf{f}}^{(t-1)}$ . The algorithm normalizes the updated precoding vector by  $\bar{\mathbf{f}}^{(t)} = \bar{\mathbf{f}}^{(t)} / \|\bar{\mathbf{f}}^{(t)}\|$ . We repeat these steps until either  $\bar{\mathbf{f}}^{(t)}$  converges to a tolerance level (e.g.  $\|\bar{\mathbf{f}}^{(t)} - \bar{\mathbf{f}}^{(t-1)}\| < \varepsilon_1$  for  $\varepsilon_1 > 0$ ) or the algorithm reaches  $t_{1,\max}$ .

### B. Optimizing RIS Phase Shifts $\Phi$

In this subsection, we put forth a multi-RIS phase-shift optimization method for given  $\mathbf{F}$ . We have two primary motivations for developing the RIS optimization method within the GPI framework. First, the GPI approach offers a significant advantage over traditional optimization methods by enabling us to identify not just any local optimal solution, but a superior local optimum. This capability enhances the overall performance of our RIS system. Second, we aim to achieve efficient scaling with multiple RISs. This is made possible by leveraging the block-diagonal structure of matrices within the GPI method, for example, (28) and (29). This structural property, which we will discuss later in Remark 1, allows us to handle multiple RISs without a prohibitive increase in computational complexity.

Unlike the precoding optimization, however, it is required to handle the unit-modulus constraint on  $\Phi$ . To this end, we first reformulate (12) to a quadratic form with respect to  $\phi_\ell$ , providing a more tractable approach in optimizing the RIS phase shifts. Using the vectorization and introducing a permutation matrix, we convert the second term of the denominator in (14) to

$$\begin{aligned}
& \sum_{i=1}^K \mathbf{f}_i^H \left( \sum_{\ell=1}^L \mathbf{E}_{k,\ell} \phi_\ell \phi_\ell^H \mathbf{E}_{k,\ell}^H \right) \mathbf{f}_i \\
&= \sum_{\ell=1}^L \sum_{i=1}^K \phi_\ell^H \left( \mathbf{f}_i^T \otimes \mathbf{I}_M \right) \text{vec} \left( \mathbf{E}_{k,\ell}^T \right)^* \left( \text{vec} \left( \mathbf{E}_{k,\ell}^T \right)^* \right)^H \left( \mathbf{f}_i^T \otimes \mathbf{I}_M \right)^H \phi_\ell \\
&= \sum_{\ell=1}^L \sum_{i=1}^K \phi_\ell^H \left( \mathbf{f}_i^T \otimes \mathbf{I}_M \right) \mathbf{P} \mathbf{e}_{k,\ell}^* \left( \mathbf{P} \mathbf{e}_{k,\ell}^* \right)^H \left( \mathbf{f}_i^T \otimes \mathbf{I}_M \right)^H \phi_\ell, \quad (30)
\end{aligned}$$

where  $\mathbf{P}$  is a permutation matrix satisfying  $\text{vec}(\mathbf{E}^T) = \mathbf{P} \text{vec}(\mathbf{E})$ . By applying (30) to the similar process of (14)-(16),

the lower bound of instantaneous SE can be reformulated as  $\tilde{R}_k^{\text{ins}}(\Phi) = \tilde{R}_k^{\text{ins}}(\mathbf{F}, \Phi)$ , where

$$\tilde{R}_k^{\text{ins}}(\Phi) = \log_2 \left( 1 + \frac{\left| \left( \sum_{\ell=1}^L \hat{\mathbf{H}}_{k,\ell}^r \phi_\ell \right)^H \mathbf{f}_k \right|^2}{\sum_{i \neq k} \left| \left( \sum_{\ell=1}^L \hat{\mathbf{H}}_{k,\ell}^r \phi_\ell \right)^H \mathbf{f}_i \right|^2 + \sum_{\ell=1}^L \phi_\ell^H \Theta_{k,\ell} \phi_\ell + \frac{\sigma^2}{P}} \right), \quad (31)$$

and  $\Theta_{k,\ell} = \sum_{i=1}^K \left( \mathbf{f}_i^T \otimes \mathbf{I}_M \right) \mathbf{P} \left( \mathbf{R}_{k,\ell}^e \right)^* \mathbf{P}^T \left( \mathbf{f}_i^T \otimes \mathbf{I}_M \right)^H$ . With given  $\mathbf{F}$ , our problem in (17) is rewritten as

$$\underset{\Phi}{\text{maximize}} \quad \sum_{k=1}^K \tilde{R}_k^{\text{ins}}(\Phi) \quad (32)$$

$$\text{subject to} \quad |\phi_{\ell,m}| = 1, \quad \forall \ell \in \mathcal{L}, \forall m \in \mathcal{M}. \quad (33)$$

Now, to resolve the challenge of the unit-modulus constraint, we introduce a regularization approach. We first stack all individual RIS elements as a vector form as

$$\vec{\phi} = \left[ \phi_1^T, \phi_2^T, \dots, \phi_L^T \right]^T = \left[ \phi_{1,1}, \phi_{1,2}, \dots, \phi_{L,M} \right]^T \in \mathbb{C}^{LM}. \quad (34)$$

We relax the unit-modulus constraint considering the difference between maximum and minimum values among all RIS phase shifts of  $\vec{\phi}$ . Then, the regularized optimization problem can be formulated without the unit-modulus constraint as

$$\underset{\Phi, \mu}{\text{maximize}} \quad \frac{1}{R_\Sigma} \sum_{k=1}^K \tilde{R}_k^{\text{ins}}(\Phi) - \frac{\mu}{\tau} \left( \max_{\substack{\ell \in \mathcal{L} \\ m \in \mathcal{M}}} |\phi_{\ell,m}|^2 - \min_{\substack{\ell \in \mathcal{L} \\ m \in \mathcal{M}}} |\phi_{\ell,m}|^2 \right), \quad (35)$$

where  $\mu$  denotes a parameter of regularization,  $\tau$  is a pre-defined normalization factor for the RIS phase shifts, and  $R_\Sigma$  is a pre-defined normalization factor for the sum SE obtained by any existing state-of-the-art precoder with randomly generated  $\Phi$ . We remark that the normalization factors are introduced to make the SE and regularization term comparable in scale, thereby reducing the effective range of  $\mu$ . In (35), the second term, commonly referred to as the penalty term, serves to enforce the unit-modulus constraint by minimizing the difference between maximum and minimum elements of  $\vec{\phi}$ . The regularization parameter  $\mu$  controls the degree of adherence to the unit-modulus constraint, ensuring that the amplitudes of relaxed RIS phase shifts remain as homogeneous as possible before projecting them into a feasible solution set, i.e., a complex unit circle.

We now tackle (35) with respect to  $\mathbf{w}$  for given  $\mu$ . To transform (35) into a more tractable form, we first normalize the RIS phase shifts vector as

$$\mathbf{w} = \frac{1}{\sqrt{LM}} \vec{\phi} = [w_1, w_2, \dots, w_{LM}]^T \in \mathbb{C}^{LM}. \quad (36)$$

With some abuse of notation, we then rewrite the objective function in (35) as

$$\mathcal{L}_{\text{RIS}}(\mathbf{w}) = \frac{1}{R_\Sigma} \sum_{k=1}^K \tilde{R}_k^{\text{ins}}(\mathbf{w}) - \frac{\mu}{\tau} \left( \max_{i=1, \dots, LM} |w_i|^2 - \min_{i=1, \dots, LM} |w_i|^2 \right). \quad (37)$$

We set  $\tau = (LM)^{-1}$  in this problem. Let us now introduce a  $LM \times LM$  diagonal matrix as

$$\mathbf{X}_i = \text{diag}(0, \dots, \underbrace{1}_{i\text{th term}}, \dots, 0), \quad i = 1, \dots, LM, \quad (38)$$

where the non-zero entry appears in  $i$ th diagonal position. By leveraging (38), we can rewrite the power of the normalized RIS phase shifts as a quadratic form as  $|w_i|^2 = \mathbf{w}^H \mathbf{X}_i \mathbf{w}$ . To transform (37) into the GPI-friendly form for  $\mathbf{w}$ , we assume  $\|\mathbf{w}\| = 1$  which is naturally true when the unit-modulus constraint is met. As a result, we can reformulate the objective function in (35) as

$$\begin{aligned} \mathcal{L}_{\text{RIS}}(\mathbf{w}) &= \frac{1}{R_\Sigma} \sum_{k=1}^K \log_2 \left( \frac{\mathbf{w}^H \mathbf{C}_k \mathbf{w}}{\mathbf{w}^H \mathbf{D}_k \mathbf{w}} \right) \\ &\quad - \frac{\mu}{\tau} \left( \max_{i=1, \dots, LM} \left\{ \mathbf{w}^H \mathbf{X}_i \mathbf{w} \right\} - \min_{i=1, \dots, LM} \left\{ \mathbf{w}^H \mathbf{X}_i \mathbf{w} \right\} \right), \end{aligned} \quad (39)$$

where

$$\mathbf{C}_k = LM \text{blkdiag}(\mathbf{Y}_{k,1} + \mathbf{\Theta}_{k,1}, \dots, \mathbf{Y}_{k,L} + \mathbf{\Theta}_{k,L}) + \frac{\sigma^2}{P} \mathbf{I}_{LM}, \quad (40)$$

$$\mathbf{D}_k = LM \text{blkdiag}(\bar{\mathbf{Y}}_{k,1} + \mathbf{\Theta}_{k,1}, \dots, \bar{\mathbf{Y}}_{k,L} + \mathbf{\Theta}_{k,L}) + \frac{\sigma^2}{P} \mathbf{I}_{LM}, \quad (41)$$

$$\mathbf{Y}_{k,\ell} = \hat{\mathbf{H}}_{k,\ell}^r \mathbf{Q} \hat{\mathbf{H}}_{k,\ell}^r, \quad \bar{\mathbf{Y}}_{k,\ell} = \hat{\mathbf{H}}_{k,\ell}^r \bar{\mathbf{Q}}_k \hat{\mathbf{H}}_{k,\ell}^r, \quad (42)$$

$$\mathbf{Q} = \sum_{i=1}^K \mathbf{f}_i \mathbf{f}_i^H, \quad \bar{\mathbf{Q}}_k = \mathbf{Q} - \mathbf{f}_k \mathbf{f}_k^H. \quad (43)$$

In (39), we need to approximate the non-smooth functions such as  $\max(\cdot)$  and  $\min(\cdot)$  for finding the optimality condition. To this end, we adopt a LogSumExp approach [44]:

$$\min_{i=1, \dots, J} \{x_i\} \approx -\alpha \ln \left( \sum_{i=1}^J \exp \left( \frac{x_i}{-\alpha} \right) \right), \quad (44)$$

$$\max_{i=1, \dots, J} \{x_i\} \approx \alpha \ln \left( \sum_{i=1}^J \exp \left( \frac{x_i}{\alpha} \right) \right), \quad (45)$$

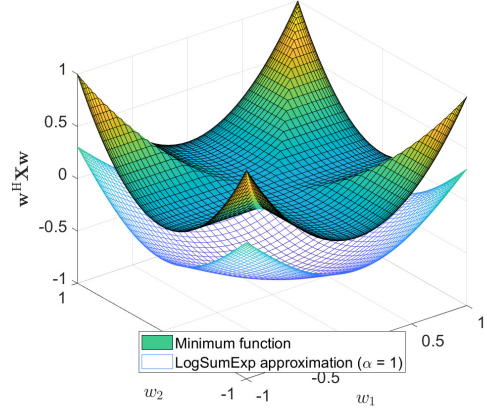
where the approximation becomes tight as  $\alpha \rightarrow +\infty$  for both cases. Using the LogSumExp, (39) is approximated as

$$\mathcal{L}_{\text{RIS}}(\mathbf{w}) \approx \tilde{\mathcal{L}}_{\text{RIS}}(\mathbf{w}) = \log_2 \lambda_{\text{RIS}}(\mathbf{w}), \quad (46)$$

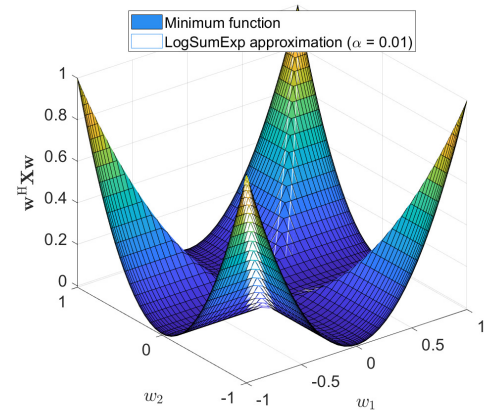
where

$$\begin{aligned} \lambda_{\text{RIS}}(\mathbf{w}) &= \prod_{k=1}^K \left( \frac{\mathbf{w}^H \mathbf{C}_k \mathbf{w}}{\mathbf{w}^H \mathbf{D}_k \mathbf{w}} \right)^{\frac{1}{R_\Sigma}} \left( \sum_{i=1}^{LM} \exp \left( \frac{\mathbf{w}^H \mathbf{X}_i \mathbf{w}}{\alpha_1} \right) \right)^{-\frac{\alpha_1 \mu \ln 2}{\tau}} \\ &\quad \times \left( \sum_{i=1}^{LM} \exp \left( \frac{\mathbf{w}^H \mathbf{X}_i \mathbf{w}}{-\alpha_2} \right) \right)^{-\frac{\alpha_2 \mu \ln 2}{\tau}}. \end{aligned} \quad (47)$$

To further illustrate the behavior of the non-smooth function used in the approximation, we present Fig. 2, which compares LogSumExp with the exact minimum function. This comparison demonstrates the trade-off in the LogSumExp approximation: a lower value of  $\alpha$  tightens the approximation accuracy yet induces steep gradients that may compromise numerical stability, whereas a higher  $\alpha$  ensures smoother gradients for stability at the cost of accuracy.



(a)  $\min(\cdot)$  vs. LogSumExp with  $\alpha = 1$



(b)  $\min(\cdot)$  vs. LogSumExp with  $\alpha = 0.01$

Fig. 2. An illustration of the comparison between the true minimum function and the LogSumExp approximation.

We further analyze the convergence properties of our GPI-based algorithm from a *fixed-point iteration perspective* [45] to rigorously explain why an extremely small value of  $\alpha$  leads to instability. Our GPI-based algorithm updates the solution iteratively using a mapping function  $\mathcal{T} : \mathbb{C}^{LM} \rightarrow \mathbb{C}^{LM}$ . Since the update rule takes the form  $\mathbf{w}^{(t+1)} = \mathcal{T}(\mathbf{w}^{(t)})$ , the algorithm constitutes a fixed-point iteration. For the algorithm to converge stably to a fixed point  $\mathbf{w}^*$ , the mapping  $\mathcal{T}$  must be a contraction mapping in the neighborhood of  $\mathbf{w}^*$ . A sufficient condition for local convergence is that the spectral radius of the Jacobian matrix of  $\mathcal{T}$  must be less than 1:

$$\rho(\mathcal{J}_{\mathcal{T}}(\mathbf{w}^*)) < 1, \quad (48)$$

where  $\mathcal{J}_{\mathcal{T}}$  indicates the Jacobian of  $\mathcal{T}$  defined as  $\mathcal{J}_{\mathcal{T}}(\mathbf{w}) = \nabla \mathcal{T}(\mathbf{w})$  and  $\rho(\cdot)$  indicates the spectral radius.

Although our GPI update is not a simple gradient descent step, we can draw a direct analogy to the standard gradient-based fixed-point iteration to understand the impact of curvature, i.e.,

$$\mathbf{w}^{(t+1)} = \mathbf{w}^{(t)} + \eta \nabla \tilde{\mathcal{L}}_{\text{RIS}}(\mathbf{w}), \quad (49)$$

where  $\eta$  is a step size. In this case, the Jacobian is governed by the Hessian of the objective function:

$$\mathcal{J}_{\mathcal{T}}(\mathbf{w}) \approx \mathbf{I} + \eta \nabla^2 \tilde{\mathcal{L}}_{\text{RIS}}(\mathbf{w}). \quad (50)$$

Stability requires that the eigenvalues of the Hessian,  $\lambda_i(\nabla^2 \tilde{\mathcal{L}}_{\text{RIS}}(\mathbf{w}))$ , are not excessively large. However, the Hessian of LogSumExp is inversely proportional to the smoothing parameter  $\alpha$  where  $\alpha = \alpha_1 = \alpha_2$ :

$$\|\nabla^2 \text{LogSumExp}(\mathbf{w}; \alpha)\| \propto \frac{1}{\alpha}. \quad (51)$$

This implies that as  $\alpha \rightarrow 0$ , the curvature of the objective function becomes arbitrarily large, i.e., forming a sharp edge. Consequently, an extremely small  $\alpha$  induces a sharp curvature in the optimization landscape. In such regions, the Jacobian  $\mathcal{J}_{\mathcal{T}}(\mathbf{w})$  typically exhibits large eigenvalues, causing the spectral radius to exceed 1 ( $\rho(\mathcal{J}_{\mathcal{T}}) > 1$ ). Under these conditions, the fixed-point iteration becomes locally expansive rather than contractive, leading to oscillations or divergence. Therefore, there exists a fundamental trade-off: while a smaller  $\alpha$  reduces the approximation error, it increases the numerical sensitivity of the problem, compromising the stability of the iterative algorithm.

Finally, the regularized optimization problem in (35) is reformulated and approximated for given  $\mu$  as

$$\underset{\mathbf{w}}{\text{maximize}} \tilde{\mathcal{L}}_{\text{RIS}}(\mathbf{w}). \quad (52)$$

Then, similar to the precoding optimization, we derive Lemma 2 for the approximated problem in (52) to find the stationary points of (47).

**Lemma 2.** *The stationary condition of (52) is also satisfied if the following holds:*

$$\bar{\mathbf{D}}^{-1}(\mathbf{w})\bar{\mathbf{C}}(\mathbf{w})\mathbf{w} = \lambda_{\text{RIS}}(\mathbf{w})\mathbf{w}, \quad (53)$$

where

$$\bar{\mathbf{C}}(\mathbf{w}) = \lambda_{\text{RIS,num}}(\mathbf{w}) \times \left[ \frac{1}{R_{\Sigma} \ln 2} \sum_{k=1}^K \left( \frac{\mathbf{C}_k}{\mathbf{w}^H \mathbf{C}_k \mathbf{w}} \right) + \frac{\mu \sum_{i=1}^{LM} \mathbf{X}_i e^{-\frac{\mathbf{w}^H \mathbf{X}_i \mathbf{w}}{\alpha_2}}}{\sum_{i=1}^{LM} e^{-\frac{\mathbf{w}^H \mathbf{X}_i \mathbf{w}}{\alpha_2}}} \right], \quad (54)$$

$$\bar{\mathbf{D}}(\mathbf{w}) = \lambda_{\text{RIS,den}}(\mathbf{w}) \times \left[ \frac{1}{R_{\Sigma} \ln 2} \sum_{k=1}^K \left( \frac{\mathbf{D}_k}{\mathbf{w}^H \mathbf{D}_k \mathbf{w}} \right) + \frac{\mu \sum_{i=1}^{LM} \mathbf{X}_i e^{-\frac{\mathbf{w}^H \mathbf{X}_i \mathbf{w}}{\alpha_1}}}{\sum_{i=1}^{LM} e^{-\frac{\mathbf{w}^H \mathbf{X}_i \mathbf{w}}{\alpha_1}}} \right]. \quad (55)$$

*Proof.* Please refer to Appendix B. ■

As discussed in Section III-A, this stationary condition can be interpreted as the generalized eigenvalue problem. Thus, the problem is transformed for finding its principal eigenvector of (53). In this regard, such eigenvector can also be found by using the GPI method to solve (53).

We describe our regularized GPI-based RIS phase-shift optimization method in Algorithm 2. The algorithm first initializes  $\bar{\boldsymbol{\phi}}$ . To optimize  $\bar{\boldsymbol{\phi}}$  with the GPI method, the algorithm builds  $\bar{\mathbf{C}}(\mathbf{w}^{(t-1)})$  and  $\bar{\mathbf{D}}(\mathbf{w}^{(t-1)})$  for given  $\mathbf{F}$ ,  $\mu$ ,  $R_{\Sigma}$ , and  $\tau$ . From the stationary condition in (53), the algorithm updates

---

**Algorithm 2:** Regularized GPI-Based RIS Phase-Shift Optimization Algorithm

---

- 1 **initialize:**  $\bar{\boldsymbol{\phi}}^{(0)} \leftarrow \boldsymbol{\Phi}^{(0)}$ .
  - 2 Set  $\mathbf{w}^{(0)} = \frac{1}{\sqrt{LM}} \bar{\boldsymbol{\phi}}^{(0)}$  and  $t = 1$ .
  - 3 **while**  $\|\mathbf{w}^{(t)} - \mathbf{w}^{(t-1)}\| > \varepsilon_2$  or  $t \leq t_{2,\max}$  **do**
  - 4     Build  $\bar{\mathbf{C}}(\mathbf{w}^{(t-1)})$  and  $\bar{\mathbf{D}}(\mathbf{w}^{(t-1)})$  with given  $\mathbf{F}$  and  $\mu$ .
  - 5     Compute  $\mathbf{w}^{(t)} = \bar{\mathbf{D}}^{-1}(\mathbf{w}^{(t-1)})\bar{\mathbf{C}}(\mathbf{w}^{(t-1)})\mathbf{w}^{(t-1)}$ .
  - 6     Normalize  $\mathbf{w}^{(t)} = \mathbf{w}^{(t)} / \|\mathbf{w}^{(t)}\|$ .
  - 7      $t \leftarrow t + 1$ .
  - 8  $\mathbf{w}^{\star} \leftarrow \mathbf{w}^{(t)}$ .
  - 9  $\bar{\boldsymbol{\phi}}^{\star} \leftarrow e^{j\arg(\mathbf{w}^{\star})}$ .
  - 10 **return**  $\boldsymbol{\Phi}^{\star} \leftarrow \bar{\boldsymbol{\phi}}^{\star}$ .
- 

$\mathbf{w}^{(t)}$  by calculating  $\mathbf{w}^{(t)} = \bar{\mathbf{D}}^{-1}(\mathbf{w}^{(t-1)})\bar{\mathbf{C}}(\mathbf{w}^{(t-1)})\mathbf{w}^{(t-1)}$  and normalizing  $\mathbf{w}^{(t)} = \mathbf{w}^{(t)} / \|\mathbf{w}^{(t)}\|$ . We repeat these steps until either  $\mathbf{w}$  converges to a tolerance level or  $t = t_{2,\max}$ . Lastly, due to the unit-modulus constraint, the optimized  $\mathbf{w}^{\star}$  is projected onto the feasible solution set by computing  $\bar{\boldsymbol{\phi}} = e^{j\arg(\mathbf{w}^{\star})}$ .

### C. Joint Optimization Algorithm

In this subsection, we propose the alternating algorithm as described in Algorithm 3 for joint optimization of the precoder and RIS phase shifts by putting together the results in Section III-A and III-B. At the beginning of Algorithm 3, the algorithm initializes the precoder and the RIS phase shifts as  $\mathbf{F}^{(0)}$  and  $\boldsymbol{\Phi}^{(0)}$  while setting the outer iteration count  $i = 1$ . Then, the algorithm computes  $R_{\Sigma}$  for given  $\mathbf{F}^{(0)}$  to normalize the penalty term in (35).

For finding an optimal value of  $\mu$ , we adopt a line search method. With the line search, the algorithm identifies the optimal value of  $\mu$  within the range of  $\mu^{(i)} \in [\mu_{\min}, \mu_{\max}]$  with  $T_{\mu}$  linearly spaced points and the increasing step  $\Delta_{\mu}$ , i.e.,  $\mu_{\max} = \mu_{\min} + \Delta_{\mu}(T_{\mu} - 1)$ , which is updated in the outer loop. In the inner loop of the algorithm, the precoder is optimized by Algorithm 1 for given  $\boldsymbol{\Phi}$ . Subsequently, using Algorithm 2, the RIS phase shifts matrix is optimized with updated  $\mathbf{F}$ . We repeat these steps until either it converges or  $t = t_{3,\max}$  in the alternating manner. For the convergence level, we compare the current solution with the previous solution as  $\frac{|f(\mathbf{F}^{(t)}, \boldsymbol{\Phi}^{(t)}) - f(\mathbf{F}^{(t-1)}, \boldsymbol{\Phi}^{(t-1)})|}{f(\mathbf{F}^{(t-1)}, \boldsymbol{\Phi}^{(t-1)})}$  where  $f(\mathbf{F}, \boldsymbol{\Phi})$  is the objective function of the original problem in (17). We use this convergence level with a tolerance threshold  $\varepsilon_3 > 0$ . To identify the optimal value of  $\mu$ , the algorithm computes  $f(\tilde{\mathbf{F}}^{(i)}, \tilde{\boldsymbol{\Phi}}^{(i)})$  at  $\mu^{(i)}$ . Consequently, the algorithm decides  $\boldsymbol{\Phi}^{\star}$  and  $\mathbf{F}^{\star}$  that maximizes  $f(\tilde{\mathbf{F}}^{(i)}, \tilde{\boldsymbol{\Phi}}^{(i)})$  for  $i = 1, \dots, N_{\mu}$ .

### D. Complexity Analysis

Now, we analyze the complexity of the proposed algorithms. The complexity of Algorithm 1 is dominated by the inversion in  $\bar{\mathbf{B}}^{-1}(\mathbf{f})$ . Since  $\bar{\mathbf{B}}(\mathbf{f})$  is a block-diagonal and symmetric matrix, we need  $\mathcal{O}(KN^3)$  instead of  $\mathcal{O}(K^3N^3)$  to obtain the inverse of  $K$  sub-matrices in  $\bar{\mathbf{B}}(\mathbf{f})$ . Hence, the total complexity of Algorithm 1 is  $\mathcal{O}(T_1KN^3)$  where  $T_1$  is the number of its

---

**Algorithm 3: GPI-Based Precoding and RIS Phase-Shift Optimization Algorithm (GPI-PRIS)**


---

```

1 initialize:  $\mathbf{F}^{(0)}$ ,  $\Phi^{(0)}$ , and  $\mu^{(0)}$ 
2 Set iteration count for outer loop  $i = 1$ .
3 Compute  $\tau = (LM)^{-1}$  and  $R_\Sigma$  with  $(\mathbf{F}^{(0)}, \Phi^{(0)})$ .
4 while  $i \leq T_\mu$  do
5   Set  $\mu^{(i)} \leftarrow \mu^{(i-1)} + \Delta_\mu \in [\mu_{\min}, \mu_{\max}]$ .
6   Set iteration count for inner loop  $t = 1$ .
7   while  $\frac{|f(\mathbf{F}^{(t)}, \Phi^{(t)}) - f(\mathbf{F}^{(t-1)}, \Phi^{(t-1)})|}{f(\mathbf{F}^{(t-1)}, \Phi^{(t-1)})} > \varepsilon_3$  or  $t \leq t_{3, \max}$  do
8      $\mathbf{F}^{(t)} \leftarrow$  Algorithm 1  $(\mathbf{F}^{(t-1)}; \Phi^{(t-1)})$ .
9      $\Phi^{(t)} \leftarrow$  Algorithm 2  $(\Phi^{(t-1)}; \mathbf{F}^{(t)}, \mu^{(i)})$ .
10     $t \leftarrow t + 1$ .
11     $\tilde{\mathbf{F}}^{(i)} \leftarrow \mathbf{F}^{(t)}$  and  $\tilde{\Phi}^{(i)} \leftarrow \Phi^{(t)}$ .
12    Compute  $f(\tilde{\mathbf{F}}^{(i)}, \tilde{\Phi}^{(i)})$ .
13     $i \leftarrow i + 1$ .
14 Select  $i^* = \arg \max_{i=1, \dots, T_\mu} f(\tilde{\mathbf{F}}^{(i)}, \tilde{\Phi}^{(i)})$ .
15 return  $\mathbf{F}^* \leftarrow \tilde{\mathbf{F}}^{(i^*)}$  and  $\Phi^* \leftarrow \tilde{\Phi}^{(i^*)}$ .

```

---

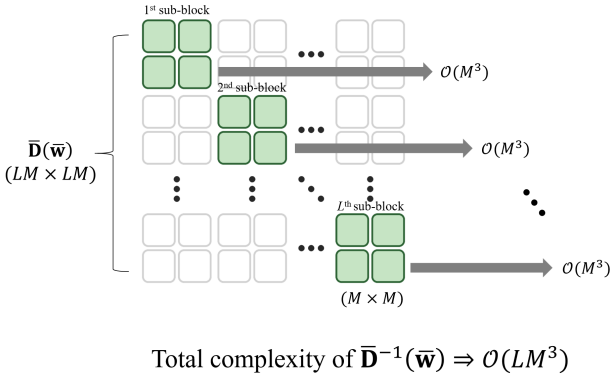


Fig. 3. An illustration of the computationally efficient matrix inversion of  $\bar{\mathbf{D}}(\bar{\mathbf{w}})$  in Algorithm 2 via block-wise decomposition.

iterations. We note that this is substantially lower compared to the existing precoding schemes. For instance, weighted mean square error (WMMSE) [46] requires  $\mathcal{O}(KN^3)$  complexity, which is the same as that of GPI-based precoding. However, GPI-based precoding accounts for the effects of channel errors by incorporating error covariance. When considering channel uncertainty, WMMSE with sample average approximation [39] requires  $\mathcal{O}((KN)^{3.5})$  complexity based on a quadratically constrained quadratic programming problem.

Similarly, Algorithm 2 complexity is dominated by the inversion in  $\bar{\mathbf{D}}^{-1}(\bar{\mathbf{w}})$  for the regularized GPI method. Since  $\bar{\mathbf{D}}(\bar{\mathbf{w}})$  is also a block-diagonal and symmetric matrix, we only need  $\mathcal{O}(LM^3)$  to obtain the inverse of each sub-matrix in  $\bar{\mathbf{D}}(\bar{\mathbf{w}})$  as depicted in Fig. 3. Accordingly, the total complexity of Algorithm 2 is  $\mathcal{O}(T_2 LM^3)$  where  $T_2$  is the number of its iterations. The state-of-the-art RIS phase-shift optimization scheme such as the MM algorithm or the MO algorithm have the complexity order of  $\mathcal{O}(M^3 + T_i M^2)$  where  $T_i$  denotes the number of iterations required for the MM algorithm or the MO

algorithm with  $i \in \{\text{MM}, \text{MO}\}$  in single-RIS-aided systems [12]. Extension to multi-RIS systems, they further need the complexity order of  $\mathcal{O}((LM)^3 + T_i(LM)^2)$  [31].

Finally, let us denote the number of iterations set for the line search of  $\mu$  as  $T_\mu$ . Then, the total complexity of Algorithm 3 (GPI-PRIS) is  $\mathcal{O}(T_\mu(T_1 KN^3 + T_2 LM^3))$ . Considering  $M > N$ , the main bottleneck arises from Algorithm 2, and the complexity becomes  $\mathcal{O}(T_\mu T_2 LM^3)$ .

**Remark 1 (Complexity Comparison and Scalability).** Our algorithm has a comparable complexity order to representative RIS optimization schemes in terms of  $M$ . However, owing to the special structure of  $\bar{\mathbf{D}}(\bar{\mathbf{w}})$ , a block-diagonal and symmetric matrix, our algorithm exhibits linear scaling with respect to  $L$ . This linear growth makes the algorithm particularly advantageous for scalable beamforming in multi-RIS-aided systems when efficient handling of a large number of RISs is essential. Particularly, it was observed that increasing the number of RISs with fixed total RIS elements  $M_{\text{tot}} = L \times M$  is advantageous up to a certain optimal  $L$  [10]. For the case of a single RIS ( $L = 1$ ) with a large number of RIS elements, the complexity of our method scales as similarly to conventional approaches, requiring a matrix inversion of size  $M_{\text{tot}} \times M_{\text{tot}}$ , which results in  $\mathcal{O}(M_{\text{tot}}^3)$  complexity. In contrast, for multi-RIS-aided systems ( $L > 1$ ), the block-diagonal structure allows us to decompose the problem into  $L$  independent sub-inversions, each corresponding to an RIS with  $M$  elements. Considering  $M = M_{\text{tot}}/L$ , the complexity of our method scales as  $\mathcal{O}(LM^3) = \mathcal{O}\left(L \cdot \left(\frac{M_{\text{tot}}}{L}\right)^3\right) = \mathcal{O}\left(\frac{M_{\text{tot}}^3}{L^2}\right)$ , allowing for flexible deployment of multiple RISs to maximize the sum SE. This is also numerically verified in Fig. 11 in Section IV-B.

### E. Reduced-Complexity Approach

While our proposed algorithm exhibits linear scalability in  $L$ , the cubic dependence on  $M$  incurs high computational cost. To mitigate this issue, we introduce a reduced-complexity GPI approach based on the framework in [47]. As a first step, we approximate  $\mathbf{C}_{k,\ell}$  by diagonal matrix:  $\mathbf{C}_{k,\ell} \approx a_{k,\ell} \mathbf{I}_{NM}$ . Here,  $a_{k,\ell}$  is the large-scale fading of user  $k$  associated with RIS  $\ell$ . Consequently, from (8), we have  $\mathbf{R}_{k,\ell}^e \approx \left(a_{k,\ell} \mathbf{I}_{NM} + \frac{T_{\text{UL}} \rho_{\text{UL}}}{\gamma_{k,\ell} \sigma^2} \mathbf{I}_{NM}\right)^{-1} = b_{k,\ell} \mathbf{I}_{NM}$ . This approximation implies that  $\Xi_{k,\ell}$  and  $\Theta_{k,\ell}$  can also be approximated as diagonal matrices. Subsequently, we reorganize the following expressions:

$$\bar{\mathbf{D}}(\bar{\mathbf{w}}) = \sum_{k=1}^K \frac{\mathbf{D}_k}{\mathbf{w}^H \mathbf{D}_k \mathbf{w}} + \mathbf{X}(\bar{\mathbf{w}}), \quad (56)$$

$$\mathbf{X}(\bar{\mathbf{w}}) = \frac{\mu}{\tau} \frac{\sum_{i=1}^{LM} \mathbf{X}_i e^{\alpha_i \mathbf{w}^H \mathbf{X}_i \mathbf{w}}}{\sum_{i=1}^{LM} e^{\alpha_i \mathbf{w}^H \mathbf{X}_i \mathbf{w}}}. \quad (57)$$

Since  $\bar{\mathbf{D}}(\bar{\mathbf{w}}) = \text{blkdiag}(\bar{\mathbf{D}}_1(\bar{\mathbf{w}}), \dots, \bar{\mathbf{D}}_L(\bar{\mathbf{w}}))$  is block-diagonal,

its  $\ell$ th sub-block is defined as

$$\begin{aligned}\bar{\mathbf{D}}_\ell(\mathbf{w}) &= \sum_{k=1}^K \frac{1}{\mathbf{w}^H \mathbf{D}_k \mathbf{w}} \left( \hat{\mathbf{H}}_{k,\ell}^r \sum_{i \neq k}^K \mathbf{f}_i \mathbf{f}_i^H \hat{\mathbf{H}}_{k,\ell}^r + \mathbf{\Theta}_{k,\ell} \right) + \mathbf{X}(\mathbf{w}) \\ &= \sum_{k=1}^K \sum_{i \neq k}^K c_k(\mathbf{w}) \mathbf{v}_{i,k,\ell} \mathbf{v}_{i,k,\ell}^H + \sum_{k=1}^K \mathbf{\Theta}_{k,\ell} + \mathbf{X}(\mathbf{w}),\end{aligned}\quad (58)$$

where  $\mathbf{v}_{i,k,\ell} = \hat{\mathbf{H}}_{k,\ell}^r \mathbf{f}_i \in \mathbb{C}^M$  and  $c_k(\mathbf{w}) = \frac{1}{\mathbf{w}^H \mathbf{D}_k \mathbf{w}}$ . Approximating each  $\mathbf{\Theta}_{k,\ell}$  by a diagonal matrix as above, we can approximate  $\bar{\mathbf{D}}_\ell(\mathbf{w})$  as

$$\bar{\mathbf{D}}_\ell(\mathbf{w}) \approx \sum_{k=1}^K \sum_{i \neq k}^K c_k(\mathbf{w}) \mathbf{v}_{i,k,\ell} \mathbf{v}_{i,k,\ell}^H + \mathbf{Y}_\ell(\mathbf{w}) = \tilde{\mathbf{D}}_\ell(\mathbf{w}), \quad (59)$$

where  $\mathbf{Y}_\ell(\mathbf{w}) = \sum_{k=1}^K \mathbf{\Theta}_{k,\ell} + \mathbf{X}(\mathbf{w})$  is a diagonal matrix. The inverse of the  $\ell$ th sub-block is given by

$$\tilde{\mathbf{D}}_\ell^{-1}(\mathbf{w}) = \left[ \sum_{k=1}^K \sum_{i \neq k}^K c_k(\mathbf{w}) \mathbf{v}_{i,k,\ell} \mathbf{v}_{i,k,\ell}^H + \mathbf{Y}_\ell(\mathbf{w}) \right]^{-1}. \quad (60)$$

By applying the Sherman-Morrison-Woodbury (SMW) formula:  $(\mathbf{A} + \mathbf{u}\mathbf{v}^H)^{-1} = \mathbf{A}^{-1} - \frac{\mathbf{A}^{-1}\mathbf{u}\mathbf{v}^H\mathbf{A}^{-1}}{1 + \mathbf{v}^H\mathbf{A}^{-1}\mathbf{u}}$ , we can easily compute the inverse of (59) in a recursive manner. Specifically, the inverse of  $\tilde{\mathbf{D}}_\ell(\mathbf{w})$  is obtained by recursively computing the previously obtained inverse via the SMW formula as

$$\begin{aligned}\tilde{\mathbf{D}}_{\ell,(p)}^{-1}(\mathbf{w}) &= \left[ \tilde{\mathbf{D}}_{\ell,(p-1)}^{-1}(\mathbf{w}) + c_{(p)}(\mathbf{w}) \mathbf{v}_{\ell,(p)} \mathbf{v}_{\ell,(p)}^H \right]^{-1} \\ &= \tilde{\mathbf{D}}_{\ell,(p-1)}^{-1}(\mathbf{w}) - \frac{c_{(p)}(\mathbf{w}) \tilde{\mathbf{D}}_{\ell,(p-1)}^{-1}(\mathbf{w}) \mathbf{v}_{\ell,(p)} \mathbf{v}_{\ell,(p)}^H \tilde{\mathbf{D}}_{\ell,(p-1)}^{-1}(\mathbf{w})}{1 + c_{(p)}(\mathbf{w}) \mathbf{v}_{\ell,(p)}^H \tilde{\mathbf{D}}_{\ell,(p-1)}^{-1}(\mathbf{w}) \mathbf{v}_{\ell,(p)}},\end{aligned}\quad (61)$$

where  $\tilde{\mathbf{D}}_{\ell,(p)}^{-1}(\mathbf{w})$  denotes the inverse obtained after the  $p$ th rank-one update in (59),  $\mathbf{v}_{\ell,(p)}$  is the  $p$ -th vector selected from the set  $\{\mathbf{v}_{i,k,\ell}, \forall i, k\}$ , and  $c_{(p)}$  is the corresponding scalar associated with  $\mathbf{v}_{\ell,(p)}$ . By using this recursively rank-one update strategy, the complexity of obtaining (59) is  $O(K(K-1)M^2)$  in a divide-and-conquer manner. Specifically, we accumulate  $K(K-1)$  rank-one updates  $\mathbf{v}_{i,k,\ell} \mathbf{v}_{i,k,\ell}^H$ , where each of which takes  $O(M^2)$  complexity. Since there are  $L$  sub-blocks, the overall complexity becomes  $O(LK(K-1)M^2)$ . For  $M \gg K$ , this typically much lower than  $O(LM^3)$  complexity of directly inverting the block-diagonal matrix  $\tilde{\mathbf{D}}(\mathbf{w})$ .

#### IV. NUMERICAL RESULTS

In this section, we present numerical comparisons between our proposed algorithms and the following baselines:

- **GPI-PRIS**: Our proposed algorithm (Algorithm 3).
- **R-GPI-PRIS**: Our proposed GPI-PRIS with the reduced-complexity approach as described in Section III-E.
- **WMMSE-MO**: The WMMSE precoder with manifold-based RIS phase shifts optimization [32].
- **WMMSE-PINet**: The WMMSE precoder with PINet-based RIS phase shifts optimization, which is a model-driven deep learning approach [48].
- **FP-SE**: A fractional programming-based sum SE maximization method by setting  $\xi = 0$  in Algorithm 3 of [49].
- **RZF-MO**: A regularized zero-forcing (RZF) precoder with manifold-based RIS phase shifts optimization [32].

- **Alg 1-MO**: Our proposed Algorithm 1 precoder with manifold-based RIS phase shifts optimization [32].
- **Alg 1-Random**: With Algorithm 1, phase shifts of each RIS are randomly selected.

We use RZF as an initial precoder of Algorithm 1. Using line search with  $T_\mu = 15$  linearly spaced points, we identify the optimal value of  $\mu$  in range  $\mu \in [0, 100]$ .

#### A. Simulation Environments

In the considered system, we assume that both antennas at the BS and elements of the RISs are arranged in uniform planar arrays (UPAs). In the presence of the same spatial paths  $L_{BR}$  for all BS-RIS links, the channel matrix between the BS and RIS  $\ell$  is given by  $\forall \ell \in \mathcal{L}$

$$\mathbf{H}_{1,\ell} = \frac{1}{\sqrt{L_{BR}}} \sum_{i=1}^{L_{BR}} \sqrt{\gamma_{1,\ell}} \mathbf{a}_B(\vartheta_{i,\ell}^a, \vartheta_{i,\ell}^e) \mathbf{a}_R^H(\varphi_{i,\ell}^a, \varphi_{i,\ell}^e), \quad (62)$$

where  $\gamma_{1,\ell}$  is the path gain of  $\ell$ th BS-RIS link,  $\vartheta_{i,\ell}^a$  ( $\varphi_{i,\ell}^a$ ) and  $\vartheta_{i,\ell}^e$  ( $\varphi_{i,\ell}^e$ ) denote azimuth and elevation of AoDs (AoAs), and  $\mathbf{a}(\cdot)$  denotes a steering vector. Considering  $N_y$  and  $N_z$  as the horizontal and vertical indices of the BS antenna, i.e.,  $N = N_y \times N_z$ , the array response vectors at the BS and RIS  $\ell$  are defined as  $\mathbf{a}_B(\vartheta_{i,\ell}^a, \vartheta_{i,\ell}^e) = \mathbf{a}_B^y(\vartheta_{i,\ell}^a, \vartheta_{i,\ell}^e) \otimes \mathbf{a}_B^z(\vartheta_{i,\ell}^e)$ ,  $\mathbf{a}_R(\varphi_{i,\ell}^a, \varphi_{i,\ell}^e) = \mathbf{a}_R^y(\varphi_{i,\ell}^a, \varphi_{i,\ell}^e) \otimes \mathbf{a}_R^z(\varphi_{i,\ell}^e)$ . The array response vectors at the BS are defined as

$$\begin{aligned}\mathbf{a}_B^y(\vartheta_{i,\ell}^a, \vartheta_{i,\ell}^e) &= \left[ 1, e^{j2\pi \frac{\Delta_B^y}{\lambda_c} \sin(\vartheta_{i,\ell}^a) \sin(\vartheta_{i,\ell}^e)}, \dots, e^{j2\pi(N_y-1) \frac{\Delta_B^y}{\lambda_c} \sin(\vartheta_{i,\ell}^a) \sin(\vartheta_{i,\ell}^e)} \right]^T, \\ \mathbf{a}_B^z(\vartheta_{i,\ell}^e) &= \left[ 1, e^{j2\pi \frac{\Delta_B^z}{\lambda_c} \cos(\vartheta_{i,\ell}^e)}, \dots, e^{j2\pi(N_z-1) \frac{\Delta_B^z}{\lambda_c} \cos(\vartheta_{i,\ell}^e)} \right]^T,\end{aligned}\quad (63)$$

where  $\Delta_B^y$  and  $\Delta_B^z$  are the distance between adjacent BS antennas along two axes. Similarly, with the horizontal and vertical dimensions of the RIS  $M_y$  and  $M_z$  (i.e.,  $M = M_y \times M_z$ ), its array response vectors,  $\mathbf{a}_R^y(\varphi_{i,\ell}^a, \varphi_{i,\ell}^e)$  and  $\mathbf{a}_R^z(\varphi_{i,\ell}^e)$ , are defined analogously to (63) and (64), respectively. We assume that the same total number of spatial paths between RIS and user is  $L_{RU}$  for all RIS-user links. The RIS-user channel is

$$\mathbf{h}_{2,k,\ell} = \frac{1}{\sqrt{L_{RU}}} \sum_{i=1}^{L_{RU}} \sqrt{\gamma_{2,k,\ell}} \alpha_{k,i,\ell}^{sc} \mathbf{a}_R(\vartheta_{k,i,\ell}^{R,a}, \vartheta_{k,i,\ell}^{R,e}), \quad (65)$$

where  $\gamma_{2,k,\ell}$  denotes the path gain of the RIS-user link,  $\alpha_{k,i,\ell}^{sc}$  denotes small-scale fading satisfying  $\alpha_{k,i,\ell}^{sc} \sim \mathcal{CN}(0, 1)$ , and  $(\vartheta_{k,i,\ell}^{R,a}, \vartheta_{k,i,\ell}^{R,e})$  denote azimuth and elevation AoDs between RIS  $\ell$  and user  $k$ .

Considering that the system operates at a 28 GHz carrier frequency, we adopt the mmWave pathloss model [50]. Thus, the pathloss in dB is given by

$$\text{PL}(d) = \alpha_{PL} + \beta_{PL} 10 \log_{10} d + \chi \text{ [dB]}, \quad (66)$$

where  $d$  denotes the link distance in meter,  $\chi \sim \mathcal{N}(0, \sigma_s^2)$  is the log-normal shadowing. This pathloss model is applied to the path gain terms in (62) and (65). According to [50],

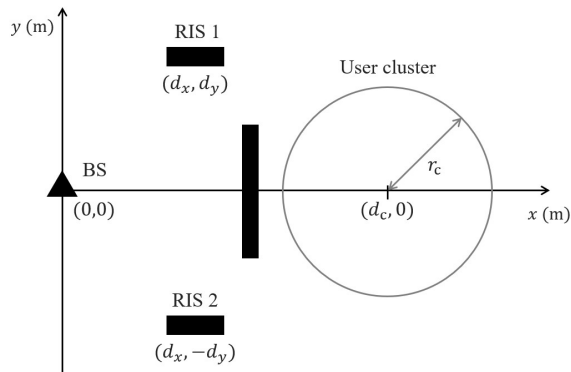


Fig. 4. A schematic of the multiuser network with two RISs

TABLE I  
COMPARISON OF SUM SE UNDER DIFFERENT LOGSUMEXP PARAMETER

$P$ (dBm)	Sum SE (bits/sec/Hz)				
	$\alpha = 0.001$	$\alpha = 0.01$	$\alpha = 0.1$	$\alpha = 1$	$\alpha = 10$
0	10.84	10.98	11.09	11.29	11.25
20	NaN	25.98	26.39	25.68	23.86
40	NaN	31.01	30.97	29.59	26.74

the experimental data for 28 GHz channels and 1 GHz bandwidth indicates that the parameters in (66) are set to be  $\alpha_{\text{PL}} = 61.4$  dB,  $\beta_{\text{PL}} = 2$  dB,  $\sigma_s^2 = 5.8$  dB. Additionally, the noise power is given by

$$P_{\text{noise}} = -174 + 10 \log_{10} W + n_f \text{ [dBm]}, \quad (67)$$

where  $W$  and  $n_f$  are the channel bandwidth and noise figure at the BS. Assuming the normalized noise variance, i.e.,  $\sigma^2 = 1$ , the large-scale path gain is computed also from normalizing the pathloss as

$$\gamma = -(\text{PL}(d) + P_{\text{noise}}) \text{ [dB]}. \quad (68)$$

In (67), we consider  $W = 1$  GHz and  $n_f = 5$  dB. In the considered channel model, we set  $\Delta_{\text{B}}/\lambda_c = \Delta_y/\lambda_c = \Delta_z/\lambda_c = 0.5$ ,  $L_{\text{BR}} = L_{\text{RU}} = 2$ , and randomly generate the signal azimuth and elevation angles of the UPA as  $(\varphi_{i,\ell}^a, \vartheta_{k,i,\ell}^{\text{R},a}) \in [-\pi, \pi)$  and  $(\varphi_{i,\ell}^e, \vartheta_{k,i,\ell}^{\text{R},e}) \in [-\pi/2, \pi/2]$ , and also the AoD of the ULA as  $\vartheta_{\ell}^{\text{B}} \in [0, \pi]$ ,  $\forall \ell, k, i$ . For the channel estimation discussed in Section II-B, we set  $T_{\text{UL}} = M$  and  $\rho_{\text{UL}} = 0$  dBm.

In the simulations, we consider the systems assisted with  $L = 2$  RISs unless mentioned otherwise. To illustrate the location of the entities in the considered system, we apply a two-dimensional (2D) coordinate system as shown in Fig. 4. The BS and origin of the circle are set as  $(0, 0)$  and  $(d_c, 0)$ , respectively. The users are randomly generated within  $r_c = 20$  m radius of a circle, and the distance between the BS and the origin of the circle is set to be  $d_c = 60$  m. The locations of RISs are set as  $(d_x, d_y)$  and  $(d_x, -d_y)$ , where  $d_x = d_y = 20$  m.

To empirically justify the setting of the smoothing parameters  $\alpha_1$  and  $\alpha_2$  in LogSumExp, we investigate their impact on the performance of GPI-PRIS. These parameters govern the fundamental trade-off between the tightness of the

TABLE II  
SIMULATION PARAMETERS

Parameter	Value
Carrier Frequency	28 GHz
Bandwidth ( $W$ )	1 GHz
Noise Figure ( $n_f$ )	5 dB
Noise Power	$-174 + 10 \log_{10} W + n_f$ dBm
Array Structure	uniform planar array (UPA)
Antenna Spacing ( $\Delta/\lambda_c$ )	0.5
BS Location	$(0, 0)$ m
User Cluster Center ( $d_c$ )	$(60, 0)$ m
User Cluster Radius ( $r_c$ )	20 m
RIS Locations	$(20, 20)$ m, $(20, -20)$ m
Path Loss Parameters	$\alpha_{\text{PL}} = 61.4, \beta_{\text{PL}} = 2, \sigma_s = 5.8$ dB
Number of Paths ( $L_{\text{BR}}, L_{\text{RU}}$ )	2
Uplink Training Length ( $T_{\text{UL}}$ )	$M$
Uplink Training Power ( $\rho_{\text{UL}}$ )	0 dBm
Maximum Iterations	$t_{1,\text{max}} = t_{2,\text{max}} = t_{3,\text{max}} = 30$
Tolerance Levels	$\epsilon_1 = \epsilon_3 = 10^{-2}, \epsilon_2 = 10^{-3}$
LogSumExp Parameters	$\alpha_1 = \alpha_2 = 0.1$
$\mu$ Search ( $T_{\mu}$ )	15 (Range: $[0, 100]$ )
Initial Precoder	RZF
Initial RIS Phase Shift	randomly generated $\phi \in [-\pi, \pi)$

approximation and the numerical stability of the algorithm. Consistent with the theoretical analysis in Section III-B, as  $\alpha \rightarrow 0$ , the LogSumExp approximation provides a tighter approximation of the non-smooth max/min functions. However, this improved accuracy comes at the cost of inducing extreme curvature in the optimization landscape. As discussed, such sharp curvature increases the spectral radius of the iteration mapping's Jacobian matrix, which can violate the contraction mapping condition essential for convergence. The results demonstrate that setting  $\alpha = 0.1$  yields the reasonably high sum SE, offering a suitable balance between approximation accuracy and stability. Conversely, reducing  $\alpha$  to 0.001 caused computational failure ('NaN' in Table I). This empirical failure confirms our theoretical insight that the loss of contraction at extremely small  $\alpha$  results in algorithm divergence. Based on these empirical findings, we adopted  $\alpha_1 = \alpha_2 = 0.1$  for all subsequent simulations.

## B. Performance Evaluation

1) *Maximum Transmit Power vs. Sum SE*: We evaluate the performance of the proposed algorithm with respect to the maximum transmit power  $P$  for  $N = 16$ ,  $K = 4$ ,  $M = 64$  ( $M_y = 8$ ,  $M_z = 8$ ). As shown in Fig. 5, our method achieves substantial SE gains compared to all baselines across all transmit power regimes. Specifically, the proposed algorithm exhibits a significant performance improvement over the random-phase scheme. In addition, RZF, due to its linear nature, shows limited performance in maximizing the sum SE. This observation suggests that SE performance can be effectively enhanced through RIS phase shift optimization. In terms of RIS phase shift optimization, our method shows significant performance improvement compared to Alg 1-MO by finding a superior local optimal solution. Consequently, our method demonstrates

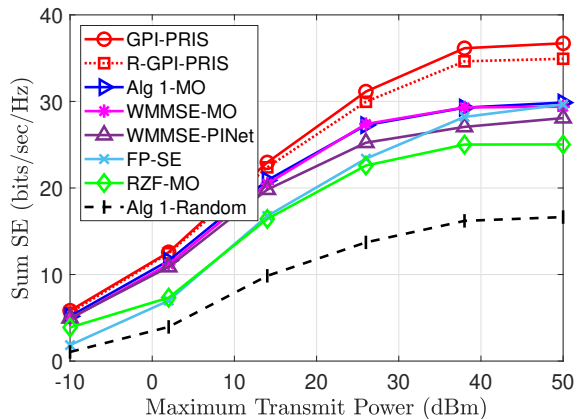


Fig. 5. The sum SE versus the maximum transmit power  $P$  dBm for  $N = 16$  BS antennas,  $K = 4$  users, and  $M = 64$  RIS phase shifts.

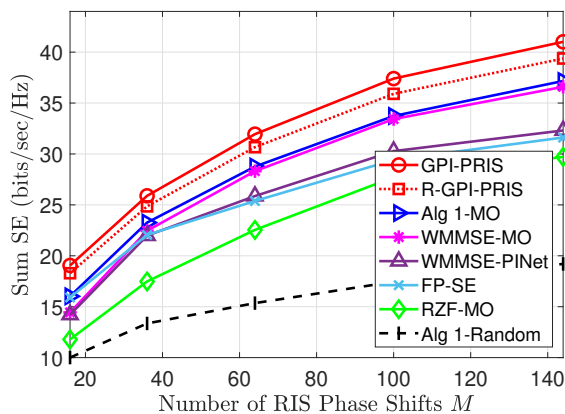


Fig. 6. The sum SE versus the number of RIS phase shifts  $M$  for  $N = 16$  BS antennas,  $K = 4$  users, and  $P = 30$  dBm maximum transmit power.

the effective joint optimization for the precoder and RIS phase shift over different transmit power regime.

2) *Number of RIS Phase Shifts vs. Sum SE*: We compare the performance of the proposed algorithm and baselines in terms of the number of RIS phase shifts  $M$  with  $M_y = M_z$ . We depict the comparison results in Fig. 6 for  $N = 16$ ,  $K = 4$ , and  $P = 30$  dBm. In Fig. 6, the proposed algorithm achieves the highest performance across all tested numbers of RIS elements. Fig. 6 also shows a significant increase in the SE performance with increasing  $M$  for our method. In contrast, the baseline methods show only marginal improvements with increasing  $M$ . This improvement is attributed to the efficient transmission strategy by properly incorporating the partial CSIT and identifying a superior local optimal point the regularized GPI method. These results emphasize the suitability of the proposed algorithm for high-speed data communications and coverage expansion by employing multiple RISs with a number of elements.

3) *CSIT Accuracy*: We investigate the sum SE in relation to the accuracy of CSIT. In this simulation, we consider  $N = 16$ ,  $K = 4$ ,  $M = 32$ , and  $P = 20$  dBm. Note that the increased value of  $\rho_{UL}$  directly correlates with improved channel estimation accuracy. As expected, Fig. 7 shows an increasing SE with  $\rho_{UL}$ . Fig. 7 demonstrates that our algo-

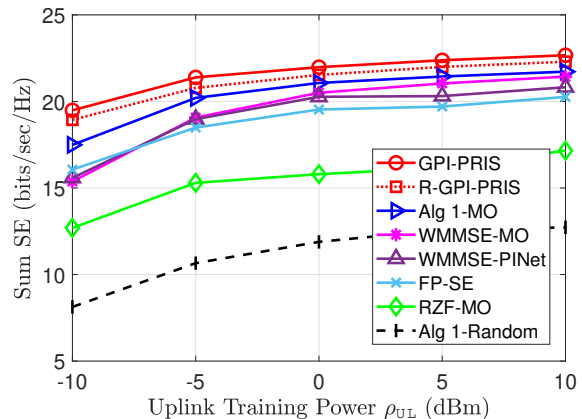
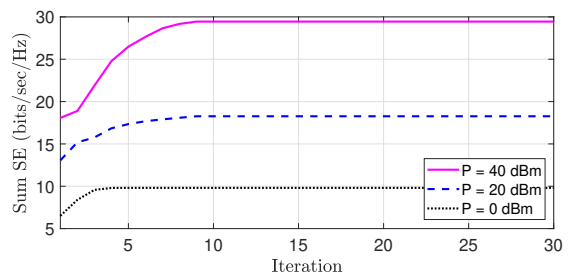
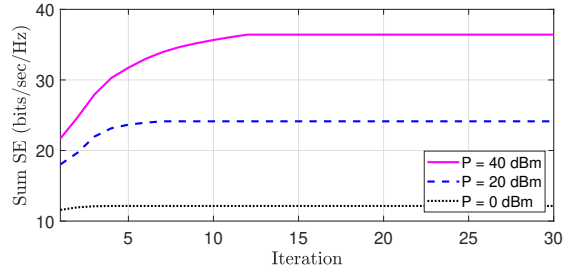


Fig. 7. The sum SE versus the channel estimation parameter  $\rho_{UL}$  for  $N = 16$  BS antennas,  $K = 4$  users,  $M = 32$  RIS phase shifts, and  $P = 20$  dBm maximum transmit power.



(a)  $M = 32$



(b)  $M = 64$

Fig. 8. Convergence behavior of GPI-PRIS (Algorithm 3) for  $N = 16$  BS antennas,  $K = 4$  users,  $M \in \{32, 64\}$  RIS phase shifts, and  $P \in \{0, 20, 40\}$  dBm maximum transmit power.

achieves the highest SE performance over different  $\rho_{UL}$ . We also observe that there exists performance gap between Alg 1-MO and WMMSE-MO in the low  $\rho_{UL}$  regime from Fig. 7. This performance gap arises from Algorithm 1 that the error covariance is embedded to effectively handle channel estimation errors. For such a reason, GPI-PRIS has robust performance in the coarse channel estimation environment owing to both Algorithm 1 and Algorithm 2 utilizing the error covariance. Thus, leveraging our GPI-based optimization framework and incorporating the error covariance-embedded transmission strategy, our algorithm offers robust joint beamforming solutions that maintain the highest performance.

4) *Convergence & Initialization Behavior*: To identify the convergence behavior of the proposed algorithm, we evaluate the proposed GPI-PRIS regarding the sum SE versus the

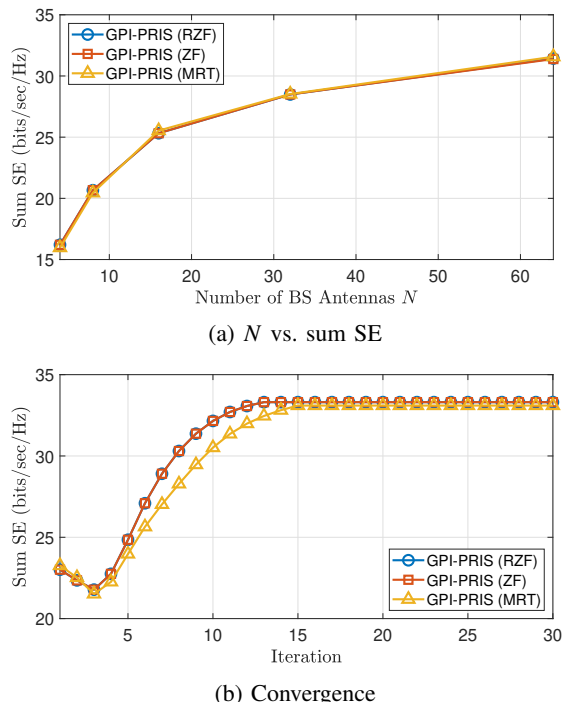


Fig. 9. The comparison of different initial precoders (RZF, ZF, and MRT) for GPI-PRIS.

number of outer iterations for the various transmit power regime as  $P \in \{0, 20, 40\}$  dBm. We assume  $N = 16$  and  $K = 4$  in both  $M = 32$  and  $M = 64$  cases. For the  $M = 32$  ( $M_y = 8, M_z = 4$ ) case, Fig. 8(a) illustrates that the proposed algorithm converges within 11 iterations. Additionally, we examine a larger scale RIS configuration with  $M = 64$  ( $M_y = 8, M_z = 8$ ) as depicted in Fig. 8(b). This scenario demonstrates that the proposed algorithm requires 13 iteration to converge. The increase in the iteration counts can be attributed to the expanded search space for the number of RIS elements. The results underscore that the proposed algorithm achieves fast convergence.

To verify the convergence stability of the proposed algorithm, we evaluated the sum SE performance under different initial precoders: RZF, zero-forcing (ZF), and maximum ratio transmission (MRT). Fig. 9(a) examines the effect of varying  $N$  while fixing  $M = 32, K = 4$ , and  $P = 40$  dBm. As shown in Fig. 9(a), the sum SE performance improves as the number of BS antennas  $N$  increases, while exhibiting negligible differences among the different initialization schemes. Furthermore, Fig. 9(b) illustrates the convergence behavior of the proposed algorithm for  $N = 16, K = 4$ , and  $M = 32$ . It is observed that despite different starting points, all initialization schemes converge to the similar steady-state sum SE value within a few iterations. This indicates that the proposed GPI-PRIS is robust to initialization and reliably converges to a superior local optimal solution without requiring careful tuning of the starting point.

5) *Regularization Behavior*: We analyze the regularization behavior of our algorithms based on a GPI method for  $N = 16$ ,

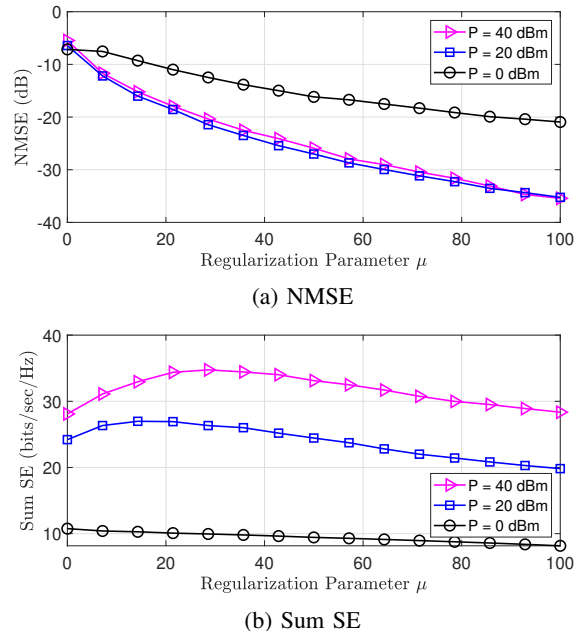


Fig. 10. The results in terms of the regularization parameter  $\mu$  for  $N = 16$  BS antennas,  $K = 4$  users,  $M = 64$  RIS phase shifts, and  $P \in \{0, 20, 40\}$  dBm maximum transmit power.

$K = 4$ , and  $M = 64$  ( $M_y = 8, M_z = 8$ ) with the following metric:

$$\text{NMSE} \left( \sqrt{LM} |\mathbf{w}^*| - \mathbf{1} \right), \quad (69)$$

where  $\text{NMSE}(\cdot)$  denotes a normalized mean square error (NMSE) function and  $\mathbf{1}$  denotes a vector whose elements are one with proper dimension. Fig. 10(a) illustrates that NMSE decreases for all transmit power regimes as  $\mu$  increases. This behavior can be attributed to the increasing dominance of the penalty term in (35) with higher  $\mu$ , which effectively enforces the unit-modulus constraint on the RIS phase shifts. Consequently, as  $\mu$  increases, NMSE approaches zero, which indicates that the unit-modulus constraint is nearly satisfied.

We also verify the SE performance with respect to the value of  $\mu$  with the same scenario considered above. In Fig. 10(b), it is observed that the sum SE is effectively maximized using the line search method. Let  $\hat{\phi}_d = [\hat{\phi}_{d,1}, \dots, \hat{\phi}_{d,L}]$  be a deviation from the optimized RIS elements prior to projecting onto the feasible solution set, which is defined as  $\hat{\phi}_d = e^{j \arg(\mathbf{w}^*)} - \sqrt{LM} \mathbf{w}^*$ . At low  $P$ , the deviation has marginal impact on SE performance, since the AWGN power is more dominant than the possible errors caused by such deviation. In this regard, the optimization primarily focuses on maximizing the sum SE with little consideration of the unit-modulus constraint. At high  $P$ , the optimization prioritizes strict adherence to the constraint, and thus the optimal  $\mu$  becomes larger. We note that depending on the transmit power, there exist optimal  $\mu$ . In addition, the sum SE reveals the low sensitivity around the optimal region. In this regard, the suitable value of  $\mu$  can be pre-defined with respect to the transmit power, which further reduces the complexity of the proposed algorithm. Overall, we confirm that our approach enables a balanced trade-off in the regularized optimization problem over  $P$ .

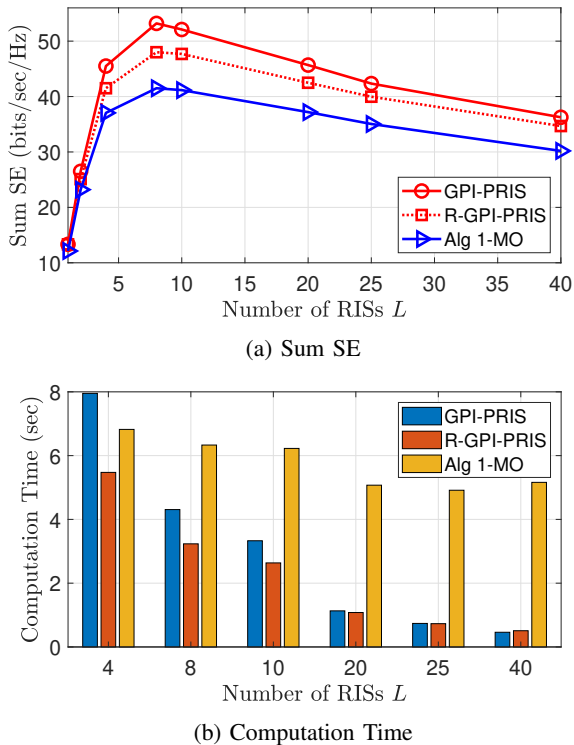


Fig. 11. The comparison of the proposed algorithms and the baseline over the number of RISs  $L$  with  $N = 32$ ,  $K = 8$ , and SNR = 20 dB. The total number of RIS elements is fixed as  $M_{\text{tot}} = LM = 200$ .

6) *Multi-RIS Scalability*: We evaluate the sum SE in scalable RIS-aided systems by increasing  $L$  and keeping the total number of deployed RIS elements  $M_{\text{tot}} = L \times M = 200$ . The values of  $M_y$  and  $M_z$  are determined such that  $M_{\text{tot}}/L = M_y \times M_z$ . We consider  $N = 32$  and  $K = 8$ . Here, we use an empirically pre-determined value of  $\mu$ , and consider only the small-scale fading with both randomly distributed RISs and users while fixing all path-loss terms as 1 for simplicity. Hence, in this scenario, we use a signal-to-noise ratio (SNR)  $P/\sigma^2$  which is set to be  $P/\sigma^2 = 20$  dB SNR. With fixed  $M_{\text{tot}}$ , Fig. 11(a) demonstrates performance improvement as  $L$  increases, reaching an optimal configuration at  $L = 8$  from the considered cases. We note that GPI-PRIS achieves the highest SE performance across different values of  $L$ .

We also assess computation time in MATLAB with the workstation (Intel i9-13900K CPU and 64GB RAM). We remark that at  $L = 8$ , where the highest sum SE is observed, GPI-PRIS achieves about 28% SE gain while requiring only about 68% computation time of Alg 1-MO. As discussed in Remark 1, GPI-PRIS exhibits complexity  $\mathcal{O}(M_{\text{tot}}^3/L^2)$ , which decreases with  $L$ , whereas Alg 1-MO has constant complexity  $\mathcal{O}(M_{\text{tot}}^2)$  independent of  $L$ . In Fig. 11(b), the computation time for GPI-PRIS decreases as  $L$  increases, while Alg 1-MO remains nearly constant, which aligns with our discussion. Furthermore, R-GPI-PRIS, with complexity  $\mathcal{O}(M_{\text{tot}}^3/L)$ , achieves even lower computation time than GPI-PRIS. Notably, at  $L = 4$ , R-GPI-PRIS requires less computation time than Alg 1-MO, while GPI-PRIS remains more computationally expensive at this point. This reduced-complexity variant ef-

fectively mitigates the computational burden for large  $M$  with only marginal performance degradation. These results offer a clearer understanding of how performance and complexity are balanced by the proposed algorithms.

Overall, our algorithm demonstrates both the superior SE performance and multi-RIS scalability compared to the baselines, which can provide significant benefit of multi-RIS systems for future wireless communications.

## V. CONCLUSION

In this paper, we proposed the scalable and effective beamforming design for multi-RIS-aided systems under imperfect CSIT. Aiming to maximize the sum SE, we reformulated the optimization problem by deriving a lower bound of the instantaneous SE with partial CSIT. Dividing the problem into two subproblems, we developed the unified GPI-based optimization framework with regularization that identifies a superior local optimal solution. In particular, by leveraging the block-diagonality of the GPI matrices, the proposed algorithm achieves multi-RIS scalability with respect to the number of RISs  $L$ , i.e.,  $\sim \mathcal{O}(1/L^2)$  for the fixed total RIS elements case. Through simulations, we showed that our method not only outperforms conventional methods in terms of SE but also demonstrates significant computational scalability with respect to the number of RISs  $L$ , making it suitable for large-scale multi-RIS deployments. Therefore, this work contributes both a robust and efficient beamforming design for practical multi-RIS-aided communication systems. For future work, it would be interesting to extend the proposed scalable framework to practical scenarios involving discrete RIS phase shifts, particularly 1-bit or 2-bit resolution phase shifts. Additionally, investigating the impact of near-field propagation in extremely large-scale RIS systems remains a promising direction for further research.

## APPENDIX A

### PROOF OF LEMMA 1

According to the stationary condition, the stationary points need to satisfy  $\partial \mathcal{L}_{\text{BS}}(\bar{\mathbf{f}})/\partial \bar{\mathbf{f}}^H = 0$ . Thus, we take the partial derivative of  $\mathcal{L}_{\text{BS}}(\bar{\mathbf{f}})$  with respect to  $\bar{\mathbf{f}}$  and set it to be zero. By using the derivative of the Rayleigh quotient form as

$$\frac{\partial \left( \frac{\bar{\mathbf{f}}^H \mathbf{A}_k \bar{\mathbf{f}}}{\bar{\mathbf{f}}^H \mathbf{B}_k \bar{\mathbf{f}}} \right)}{\partial \bar{\mathbf{f}}^H} = 2 \left( \frac{\bar{\mathbf{f}}^H \mathbf{A}_k \bar{\mathbf{f}}}{\bar{\mathbf{f}}^H \mathbf{B}_k \bar{\mathbf{f}}} \right) \left[ \frac{\mathbf{A}_k \bar{\mathbf{f}}}{\bar{\mathbf{f}}^H \mathbf{A}_k \bar{\mathbf{f}}} - \frac{\mathbf{B}_k \bar{\mathbf{f}}}{\bar{\mathbf{f}}^H \mathbf{B}_k \bar{\mathbf{f}}} \right], \quad (70)$$

we can calculate the partial derivative of  $\mathcal{L}_{\text{BS}}(\bar{\mathbf{f}})$  in (26) as

$$\frac{\partial \mathcal{L}_{\text{BS}}(\bar{\mathbf{f}})}{\partial \bar{\mathbf{f}}^H} = \sum_{k=1}^K \frac{2}{\ln 2} \left( \frac{\mathbf{A}_k \bar{\mathbf{f}}}{\bar{\mathbf{f}}^H \mathbf{A}_k \bar{\mathbf{f}}} - \frac{\mathbf{B}_k \bar{\mathbf{f}}}{\bar{\mathbf{f}}^H \mathbf{B}_k \bar{\mathbf{f}}} \right). \quad (71)$$

Using (71) the stationary condition holds if

$$\sum_{k=1}^K \left( \frac{\mathbf{A}_k}{\bar{\mathbf{f}}^H \mathbf{A}_k \bar{\mathbf{f}}} \right) \bar{\mathbf{f}} = \sum_{k=1}^K \left( \frac{\mathbf{B}_k}{\bar{\mathbf{f}}^H \mathbf{B}_k \bar{\mathbf{f}}} \right) \bar{\mathbf{f}}. \quad (72)$$

The stationary condition can be regarded as the generalized eigenvalue problem with its corresponding matrices  $\bar{\mathbf{A}}(\bar{\mathbf{f}})$  and  $\bar{\mathbf{B}}(\bar{\mathbf{f}})$  defined in (28) and (29):

$$\bar{\mathbf{A}}(\bar{\mathbf{f}})\bar{\mathbf{f}} = \lambda_{\text{BS}}(\bar{\mathbf{f}})\bar{\mathbf{B}}(\bar{\mathbf{f}})\bar{\mathbf{f}}. \quad (73)$$

Here,  $\lambda_{\text{BS,num}}(\bar{\mathbf{f}})$  and  $\lambda_{\text{BS,den}}(\bar{\mathbf{f}})$  can be any function such that  $\lambda_{\text{BS}}(\bar{\mathbf{f}}) = \lambda_{\text{BS,num}}(\bar{\mathbf{f}})/\lambda_{\text{BS,den}}(\bar{\mathbf{f}})$ . We note that  $\bar{\mathbf{B}}(\mathbf{w})$  can be considered to be invertible. This completes the proof. ■

#### APPENDIX B PROOF OF COROLLARY 2

Using the LogSumExp approach in III-B, the Lagrangian function of the problem (52) is expressed as  $\tilde{\mathcal{L}}_{\text{RIS}}(\mathbf{w})$  in (46). To find the stationary points, we take derivatives of (46) as

$$\begin{aligned} \frac{\partial \tilde{\mathcal{L}}_{\text{RIS}}(\mathbf{w})}{\partial \mathbf{w}^H} &= \frac{2}{R_\Sigma \ln 2} \sum_{k=1}^K \left[ \frac{\mathbf{C}_k \mathbf{w}}{\mathbf{w}^H \mathbf{C}_k \mathbf{w}} - \frac{\mathbf{D}_k \mathbf{w}}{\mathbf{w}^H \mathbf{D}_k \mathbf{w}} \right] \\ &- \frac{2\mu}{\tau} \frac{\sum_{m=1}^M \mathbf{X}_m \mathbf{w} e^{\mathbf{w}^H \mathbf{X}_m \mathbf{w}}}{\sum_{m=1}^M e^{\mathbf{w}^H \mathbf{X}_m \mathbf{w}}} + \frac{2\mu}{\tau} \frac{\sum_{m=1}^M \mathbf{X}_m \mathbf{w} e^{-\frac{\mathbf{w}^H \mathbf{X}_m \mathbf{w}}{\alpha_2}}}{\sum_{m=1}^M e^{-\frac{\mathbf{w}^H \mathbf{X}_m \mathbf{w}}{\alpha_2}}}. \end{aligned} \quad (74)$$

Similar to the proof of Lemma 1, we find the condition for  $\partial \tilde{\mathcal{L}}_{\text{RIS}}(\mathbf{w})/\partial \mathbf{w}^H = 0$ . Consequently, from (74), the stationary condition can be reformulated as

$$\bar{\mathbf{C}}(\mathbf{w})\mathbf{w} = \lambda_{\text{RIS}}(\mathbf{w})\bar{\mathbf{D}}(\mathbf{w})\mathbf{w}, \quad (75)$$

where its corresponding matrices  $\bar{\mathbf{C}}(\mathbf{w})$  and  $\bar{\mathbf{D}}(\mathbf{w})$  are defined in (54) and (55). Here,  $\lambda_{\text{RIS,num}}(\mathbf{w})$  and  $\lambda_{\text{RIS,den}}(\mathbf{w})$  can be any function such that  $\lambda_{\text{RIS}}(\mathbf{w}) = \lambda_{\text{RIS,num}}(\mathbf{w})/\lambda_{\text{RIS,den}}(\mathbf{w})$ . We note that  $\bar{\mathbf{D}}(\mathbf{w})$  can be considered to be invertible. ■

#### REFERENCES

- [1] Y. Liu, X. Liu, X. Mu, T. Hou, J. Xu, M. Di Renzo, and N. Al-Dhahir, "Reconfigurable intelligent surfaces: Principles and opportunities," *IEEE Comm. Surveys & Tutorials*, vol. 23, no. 3, pp. 1546–1577, 2021.
- [2] R. W. Heath, N. Gonzalez-Prelcic, S. Rangan, W. Roh, and A. M. Sayeed, "An overview of signal processing techniques for millimeter wave MIMO systems," *IEEE J. Sel. Topics Signal Process.*, vol. 10, no. 3, pp. 436–453, 2016.
- [3] P. Wang, J. Fang, L. Dai, and H. Li, "Joint transceiver and large intelligent surface design for massive MIMO mmWave systems," *IEEE Trans. Wireless Commun.*, vol. 20, no. 2, pp. 1052–1064, 2020.
- [4] Y. Lin, S. Jin, M. Matthaiou, and X. You, "Channel estimation and user localization for IRS-assisted MIMO-OFDM systems," *IEEE Trans. Wireless Commun.*, vol. 21, no. 4, pp. 2320–2335, 2021.
- [5] J. Yao, J. Xu, W. Xu, D. W. K. Ng, C. Yuen, and X. You, "Robust beamforming design for RIS-aided cell-free systems with CSI uncertainties and capacity-limited backhaul," *IEEE Trans. Commun.*, vol. 71, no. 8, pp. 4636–4649, 2023.
- [6] W. Mei, B. Zheng, C. You, and R. Zhang, "Intelligent reflecting surface-aided wireless networks: From single-reflection to multireflection design and optimization," *Proc. of the IEEE*, vol. 110, no. 9, pp. 1380–1400, 2022.
- [7] Y. Han, S. Zhang, L. Duan, and R. Zhang, "Cooperative double-IRS aided communication: Beamforming design and power scaling," *IEEE Wireless Commun. Lett.*, vol. 9, no. 8, pp. 1206–1210, 2020.
- [8] M. Aldababsa, A. M. Salhab, A. A. Nasir, M. H. Samuh, and D. B. da Costa, "Multiple RISs-aided networks: Performance analysis and optimization," *IEEE Trans. Veh. Technol.*, vol. 72, no. 6, pp. 7545–7559, 2023.
- [9] G.-H. Li, D.-W. Yue, S.-N. Jin, and Q. Hu, "Performance analysis of multi-RIS-aided mmWave MIMO systems using Poisson point processes," *IEEE Signal Process. Lett.*, 2023.
- [10] B. Al-Nahhas, M. Obeed, A. Chaaban, and M. J. Hossain, "Performance of multi-RIS-aided cell-free massive MIMO: Do more RISs always help?" *IEEE Trans. on Commun.*, 2024.
- [11] Z. Li, M. Hua, Q. Wang, and Q. Song, "Weighted sum-rate maximization for multi-IRS aided cooperative transmission," *IEEE Wireless Commun. Lett.*, vol. 9, no. 10, pp. 1620–1624, 2020.
- [12] C. Pan, H. Ren, K. Wang, W. Xu, M. Elkashlan, A. Nallanathan, and L. Hanzo, "Multicell MIMO communications relying on intelligent reflecting surfaces," *IEEE Trans. Wireless Commun.*, vol. 19, no. 8, pp. 5218–5233, 2020.
- [13] H. Huang, Y. Zhang, H. Zhang, Z. Zhao, C. Zhang, and Z. Han, "Multi-IRS-aided millimeter-wave multi-user MISO systems for power minimization using generalized Benders decomposition," *IEEE Trans. Wireless Commun.*, 2023.
- [14] Z. Chen, G. Chen, X. Y. Zhang, J. Tang, S. Jin, K.-K. Wong, and J. Chambers, "Joint Power Allocation and Phase Shifts Design for Distributed RIS-assisted Multiuser Systems," *IEEE Trans. on Mobile Comput.*, 2025.
- [15] H. Do, N. Lee, and A. Lozano, "Line-of-sight MIMO via intelligent reflecting surface," *IEEE Trans. Wireless Commun.*, 2022.
- [16] Z. Zheng, W. Jing, Z. Lu, Q. Wu, H. Zhang, and D. Gesbert, "Co-operative multi-satellite and multi-RIS beamforming: Enhancing LEO SatCom and mitigating LEO-GEO intersystem interference," *IEEE J. Sel. Areas Commun.*, 2024.
- [17] X. Li, H. Wang, Y. Chen, and S. Sheng, "Joint resource allocation and reflecting precoding design for RIS-assisted ISAC systems," *IEEE Wireless Commun. Lett.*, 2024.
- [18] M. Toka, B. Lee, J. Seong, A. Kaushik, J. Lee, J. Lee, N. Lee, W. Shin, and H. V. Poor, "RIS-Empowered LEO satellite networks for 6G: promising usage scenarios and future directions," *arXiv preprint arXiv:2402.07381*, 2024.
- [19] G. Zhou, C. Pan, H. Ren, K. Wang, and A. Nallanathan, "A framework of robust transmission design for IRS-aided MISO communications with imperfect cascaded channels," *IEEE Trans. Signal Process.*, vol. 68, pp. 5092–5106, 2020.
- [20] Y. Omid, S. M. Shahabi, C. Pan, Y. Deng, and A. Nallanathan, "Low-complexity robust beamforming design for IRS-aided MISO systems with imperfect channels," *IEEE Commun. Lett.*, vol. 25, no. 5, pp. 1697–1701, 2021.
- [21] P. Zeng, D. Qiao, H. Qian, and Q. Wu, "Joint beamforming design for IRS aided multiuser MIMO with imperfect CSI," *IEEE Trans. Veh. Technol.*, vol. 71, no. 10, pp. 10729–10743, 2022.
- [22] Y. Omid, S. M. Shahabi, C. Pan, Y. Deng, and A. Nallanathan, "Robust beamforming design for an IRS-aided NOMA communication system with CSI uncertainty," *IEEE Trans. Wireless Commun.*, vol. 23, no. 2, pp. 874–889, 2023.
- [23] W. Jiang, P. Xiong, J. Nie, Z. Ding, C. Pan, and Z. Xiong, "Robust design of IRS-aided multi-group multicast system with imperfect CSI," *IEEE Trans. Wireless Commun.*, 2023.
- [24] A. Wasfi, M. Yaseen, F. Awwad, and S. S. Ikki, "Unified Mathematical Framework for Channel Estimation in VLC Systems With Signal-Dependent Noise," *IEEE Commun. Lett.*
- [25] G. Zhou, C. Pan, H. Ren, K. Wang, and A. Nallanathan, "Intelligent reflecting surface aided multigroup multicast MISO communication systems," *IEEE Trans. Signal Process.*, vol. 68, pp. 3236–3251, 2020.
- [26] S. Zargari, A. Khalili, and R. Zhang, "Energy efficiency maximization via joint active and passive beamforming design for multiuser MISO IRS-aided SWIPT," *IEEE Wireless Commun. Lett.*, vol. 10, no. 3, pp. 557–561, 2020.
- [27] Y. Xiu, Y. Zhao, Y. Liu, J. Zhao, O. Yagan, and N. Wei, "IRS-assisted millimeter wave communications: Joint power allocation and beamforming design," in *Proc. IEEE Wireless Commun. and Netw. Conf. IEEE*, 2021, pp. 1–6.
- [28] C. Pan, G. Zhou, K. Zhi, S. Hong, T. Wu, Y. Pan, H. Ren, M. Di Renzo, A. L. Swindlehurst, R. Zhang *et al.*, "An overview of signal processing techniques for RIS/IRS-aided wireless systems," *IEEE J. Sel. Topics Signal Process.*, 2022.
- [29] E. Shtaiwi, H. Zhang, A. Abdelhadi, A. L. Swindlehurst, Z. Han, and H. V. Poor, "Sum-rate maximization for RIS-assisted integrated sensing and communication systems with manifold optimization," *IEEE Trans. Commun.*, 2023.
- [30] J. Wang, S. Gong, Q. Wu, and S. Ma, "RIS-aided MIMO systems with hardware impairments: Robust beamforming design and analysis," *IEEE Trans. Wireless Commun.*, vol. 22, no. 10, pp. 6914–6929, 2023.
- [31] S.-H. Yoon, B. Lim, M. Vu, and Y.-C. Ko, "Joint user selection and beamforming design for multi-IRS aided internet-of-things networks," *IEEE Trans. Veh. Technol.*, 2023.
- [32] H. Guo, Y.-C. Liang, J. Chen, and E. G. Larsson, "Weighted sum-rate maximization for reconfigurable intelligent surface aided wireless networks," *IEEE Trans. Wireless Commun.*, vol. 19, no. 5, pp. 3064–3076, 2020.
- [33] J. Choi, N. Lee, S.-N. Hong, and G. Caire, "Joint user selection, power allocation, and precoding design with imperfect CSIT for multi-cell MU-MIMO downlink systems," *IEEE Trans. Wireless Commun.*, vol. 19, no. 1, pp. 162–176, 2019.
- [34] J. Yao, J. Xu, W. Xu, C. Yuen, and X. You, "Superimposed RIS-phase modulation for MIMO communications: A novel paradigm of

- information transfer," *IEEE Trans. Wireless Commun.*, vol. 23, no. 4, pp. 2978–2993, 2023.
- [35] N. K. Kundu and M. R. McKay, "Channel estimation for reconfigurable intelligent surface aided MISO communications: From LMMSE to deep learning solutions," *IEEE Open Jour. of the Commun. Society*, vol. 2, pp. 471–487, 2021.
- [36] C. Xu, J. An, T. Bai, S. Sugiura, R. G. Maunder, Z. Wang, L.-L. Yang, and L. Hanzo, "Channel estimation for reconfigurable intelligent surface assisted high-mobility wireless systems," *IEEE Trans. Veh. Technol.*, vol. 72, no. 1, pp. 718–734, 2022.
- [37] E. Basar, G. C. Alexandropoulos, Y. Liu, Q. Wu, S. Jin, C. Yuen, O. A. Dobre, and R. Schober, "Reconfigurable intelligent surfaces for 6G: Emerging hardware architectures, applications, and open challenges," *IEEE Veh. Tech. Mag.*, 2024.
- [38] X. Wei, D. Shen, and L. Dai, "Channel estimation for RIS assisted wireless communications—Part I: Fundamentals, solutions, and future opportunities," *IEEE Commun. Lett.*, vol. 25, no. 5, pp. 1398–1402, 2021.
- [39] H. Joudeh and B. Clerckx, "Sum-rate maximization for linearly precoded downlink multiuser MISO systems with partial CSIT: A rate-splitting approach," *IEEE Trans. Commun.*, vol. 64, no. 11, pp. 4847–4861, 2016.
- [40] S. Lee, E. Choi, and J. Choi, "Max-Min Fairness Precoding for Physical Layer Security With Partial Channel Knowledge," *IEEE Wireless Commun. Lett.*, vol. 12, no. 9, pp. 1637–1641, 2023.
- [41] B. Hassibi and B. M. Hochwald, "How much training is needed in multiple-antenna wireless links?" *IEEE Trans. Inf. Theory*, vol. 49, no. 4, pp. 951–963, 2003.
- [42] S. Park, A. Alkhateeb, and R. W. Heath, "Dynamic subarrays for hybrid precoding in wideband mmWave MIMO systems," *IEEE Trans. Wireless Commun.*, vol. 16, no. 5, pp. 2907–2920, 2017.
- [43] J. Choi, J. Park, and N. Lee, "Energy efficiency maximization precoding for quantized massive MIMO systems," *IEEE Trans. Wireless Commun.*, vol. 21, no. 9, pp. 6803–6817, 2022.
- [44] C. Shen and H. Li, "On the dual formulation of boosting algorithms," *IEEE Trans. Pattern Analysis and Machine Intelligence*, vol. 32, no. 12, pp. 2216–2231, 2010.
- [45] Y. Nesterov, "Smooth minimization of non-smooth functions," *Mathematical programming*, vol. 103, no. 1, pp. 127–152, 2005.
- [46] Q. Shi, M. Razaviyayn, Z.-Q. Luo, and C. He, "An iteratively weighted MMSE approach to distributed sum-utility maximization for a MIMO interfering broadcast channel," *IEEE Trans. Signal Process.*, vol. 59, no. 9, pp. 4331–4340, 2011.
- [47] M. Oh, S. Yoo, N. Lee, and J. Choi, "Generalized Power Iteration-Based Precoding With Low-Complexity Matrix Inversion Approaches for Massive MIMO Systems," *IEEE Trans. Veh. Technol.*, 2025.
- [48] W. Jin, J. Zhang, C.-K. Wen, S. Jin, X. Li, and S. Han, "Low-complexity joint beamforming for RIS-assisted MU-MISO systems based on model-driven deep learning," *IEEE Trans. Wireless Commun.*, vol. 23, no. 7, pp. 6968–6982, 2023.
- [49] C. Huang, A. Zappone, G. C. Alexandropoulos, M. Debbah, and C. Yuen, "Reconfigurable intelligent surfaces for energy efficiency in wireless communication," *IEEE Trans. Wireless Commun.*, vol. 18, no. 8, pp. 4157–4170, 2019.
- [50] M. R. Akdeniz, Y. Liu, M. K. Samimi, S. Sun, S. Rangan, T. S. Rappaport, and E. Erkip, "Millimeter wave channel modeling and cellular capacity evaluation," *IEEE J. Sel. Areas Commun.*, vol. 32, no. 6, pp. 1164–1179, 2014.